Pergamon

Int. J. Solids Structures Vol. 31, No. 8, pp. 1149–1178, 1994

0020–7683/94 $6.00 + .00

PLANE STRAIN BUCKLING AND WRINKLING OF NEO-HOOKEAN LAMINATES

YUE QIU, SANGWOO KIM and THOMAS J. PENCE
Department of Materials Science and Mechanics, Michigan State University, East Lansing, MI 48824-1226, U.S.A.

(*Received* 11 *March* 1993, *no revision*)

Abstract—The buckling of layered plates is examined in the context of finite deformation incompressible nonlinear elasticity. Previous work has shown how buckled configurations are modified, and buckling loads reordered, for those buckled states that are natural extensions of previously known solutions corresponding to an isolated single neo-Hookean layer. Here we examine the possibility of new solutions that have no such isolated layer counterparts. In addition to two families that are extensions of isolated layer solutions, we find two additional families of buckled configurations for the case of a symmetric three-ply laminate and we find one additional family of buckled configurations for the case of a two-ply laminate. All of these new families of solutions have an associated wrinkling load which is a function of the stiffness ratio of the two neo-Hookean materials which form the individual layers. This new wrinkling load is higher than that of the wrinkling load associated with the previously known buckled solutions.

1. INTRODUCTION

The buckling behavior of nonlinearly elastic layered structures can depart significantly from that of a single isolated layer. As regards the latter, Sawyers and Rivlin (1974, 1982) employed the theory of small deformations superposed onto finite deformation (Biot, 1965) to determine buckling loads leading to plane strain inhomogeneous deformations in thick rectangular (single layer) plates. Their analysis, which applies to a fairly general class of isotropic incompressible nonlinearly elastic materials, indicated that the associated buckling can occur in either flexural or barrelled mode shapes with any integer number m of half-wavelength ripples in the direction of thrust. Furthermore the buckling loads associated with the onset of these various deformations are ordered sequentially with the ripple number m, beginning with $m = 1$ flexure and proceeding to $m = \infty$ flexure, which occurs at a finite value of buckling load and so is identified as a *wrinkling instability*. At even greater loads the barrelling deformations are initiated, beginning at $m = \infty$ barrelling (at the same wrinkling load) and then proceeding in reverse order toward $m = 1$ barrelling at the largest value of load.

The intricate nature of buckling in elastic multi-layers has received attention dating back to studies by Biot (1968) who identified highly localized buckling deformations in layered linearly elastic materials. An extension of the work of Sawyers and Rivlin to layered structures, with the determination of the onset of buckling analysed within the fully nonlinear theory of finite elastic deformations, was given in Pence and Song (1991) for the special case of a symmetric three-ply construction composed of two neo-Hookean constituents. Even within this specialized context, it was shown that the buckling behavior could depart significantly from that of the isolated layer. Here, as for the isolated layer, the symmetry of the construction once again leads to buckling deformations that are either flexural or barrelling in character. However certain constructions did not involve a sequential correlation of buckling load with the ripple number. An examination of the reordering of these extended isolated layer buckled solutions, i.e. the natural continuation of the solutions previously obtained by Sawyers and Rivlin (1974), was the primary subject of Pence and Song (1991). As anticipated, if the various parameters characterizing the composite construction tend to special values associated with isolated layer noncomposite construction, then the results of Pence and Song (1991) reduce to those of Sawyers and Rivlin (1974). However for values of these *composite characterization parameters* far away from the special noncomposite values, the reordering of the buckling loads could be quite

drastic, including constructions in which the $m = \infty$ wrinkling instability had the lowest buckling load, thereby rendering it the critical instability. Some consequences of these results related to optimal design of symmetric three-ply plates against these buckling instabilities were then addressed in Song and Pence (1992).

However left unaddressed in both Pence and Song (1991) and Song and Pence (1992) is the possibility of completely new buckled deformations in the multi-layered construction, by which we mean buckled deformations which have no counterpart in the noncomposite case of the isolated layer. By definition, if such solutions exist for certain layered constructions, they must cease to exist at those special values of the composite characterization parameters associated with noncomposite construction.

In this paper, we investigate the possibility of such new solutions, for rectangular plates composed of alternating neo-Hookean layers. Attention is focussed on symmetric three-ply constructions (the subject of Pence and Song, 1991), and on two-ply constructions. As shown in the next section, a general N-ply construction leads to a bifurcation condition for the onset of buckling that is found by requiring that the determinant of a $4N \times 4N$ matrix must vanish. This matrix condition stems from $4N$ boundary and interface conditions that are not trivially satisfied for the plane strain buckled solution forms under consideration. In Section 3, the symmetric three-ply construction is considered, in which case symmetry reduces the general 12×12 matrix to two separate 6×6 matrices, one of which governs flexure, and the other of which governs barrelling. For each of these two deformation types, there is a continuation of the isolated layer solutions as previously found in Pence and Song (1991), however, in addition we also uncover the existence of a completely new family of solutions for both flexure and barrelling which have no isolated layer counterpart. The buckling loads associated with these new solutions are found to be higher than those associated with the previously known solution families. In particular, the new solutions also have an associated wrinkling load which is shown to be higher than that of the wrinkling load for the previously known solutions. In fact the analysis that is developed to obtain these new families of solutions clarifies the dependence of both new and old wrinkling loads on the composite characterization parameters that specify the three-ply construction.

Section 4 is devoted to the two-ply problem. Here lack of symmetry does not permit any reduction in the general 8×8 system governing bifurcation, consequently buckling is neither of pure flexure nor pure barrelling type. In this case we obtain three families of buckled solutions. Two of these families are the extension of the isolated layer families to the two-ply case, and as such these two families have a common wrinkling load. The third family has no isolated layer counterpart, and its wrinkling load is higher than that of the other two families. The results of Section 3 and 4 prompt us to conjecture that, in general, there will be $N+1$ families of buckled solutions for the N-ply construction. The mixed mode (flexure/barrelling) nature of the buckling deformation in the two-ply case is examined in Section 5. We propose a decomposition of the general mixed mode deformation into four parts: smooth flexure, smooth barrelling, residual flexure and residual barrelling and investigate how their associated percentages vary with the ripple number m. The residual flexure and residual barrelling portions of the deformation are shown to correlate directly with the discontinuity in various high order displacement derivatives across the ply interface.

2. GENERAL FORMULATION FOR PLANE STRAIN BUCKLING

We consider an N-ply rectangular plate in which the plies are stacked along the X_2-axis. Each ply is composed of one of two neo-Hookean materials, with shear moduli $\mu^{(I)}$ and $\mu^{(II)}$, respectively, which strictly alternate by ply. The plate occupies a region $\mathscr{B}$ in its undeformed configuration, where $\mathscr{B}$ is given by

$$-l_1 \leqslant X_1 \leqslant l_1, \quad -R_1 \leqslant X_2 \leqslant R_2, \quad -l_3 \leqslant X_3 \leqslant l_3, \tag{1}$$

with $R_1 + R_2 = 2l_2$. Perfect bonding is assumed across the ply interfaces. The deformation field and the corresponding deformation gradient tensor are written as

$$\mathbf{x} = \mathbf{x}(\mathbf{X}), \quad \mathbf{F} = \frac{\partial \mathbf{x}}{\partial \mathbf{X}}, \quad \forall \mathbf{X} \in \mathscr{B}. \tag{2}$$

The incompressibility of the two neo-Hookean materials then gives the constraint

$$\det \mathbf{F} = 1. \tag{3}$$

The Piola-Kirchoff stress tensor is given by

$$\mathbf{s} = -p\mathbf{F}^{-1} + \mu^{(j)}\mathbf{F}^T, \quad j = \text{I or II for material I or II}, \tag{4}$$

where $p = p(\mathbf{X})$ is the associated hydrostatic pressure field; the equilibrium equations are

$$\operatorname{div} \mathbf{s}^T = \mathbf{0}. \tag{5}$$

In the buckling problem considered here, frictionless normal thrusts act on the two surfaces at $X_1 = \pm l_1$ yielding

$$s_{12} = s_{13} = 0, \quad x_1 = \pm \rho l_1, \quad \text{on } X_1 = \pm l_1. \tag{6}$$

Here ρ is the overall imposed stretch in the X_1 direction; the compressive case of interest corresponds to $0 < \rho < 1$. The surfaces at $X_2 = -R_1, R_2$ are taken to be traction free:

$$s_{21} = s_{22} = s_{23} = 0, \quad \text{on } X_2 = -R_1, R_2, \tag{7}$$

while the surfaces at $X_3 = \pm l_3$ are constrained to remain in their original planes by a frictionless clamp:

$$s_{31} = s_{32} = 0, \quad x_3 = \pm l_3, \quad \text{on } X_3 = \pm l_3. \tag{8}$$

Across each interface of the N-ply plate, both tractions and displacements are continuous due to the assumption of perfect bonding:

$$s_{2i}|_{X_2^+} = s_{2i}|_{X_2^-}, \quad \mathbf{x}|_{X_2^+} = \mathbf{x}|_{X_2^-}, \quad (i = 1, 2, 3) \quad \text{on interfaces}, \tag{9}$$

where $X_2 = X_2^{(k)}$, $k = 1, 2, \ldots, N-1$ are the ply interface locations.

The governing equations (5) with (4), the incompressibility constraint (3), the boundary conditions (6)–(8) and the interface conditions (9) constitute a complete boundary value problem, which, to within a rigid body translation in the X_2-direction, has exactly one pure homogeneous solution as follows:

$$x_1 = \rho X_1, \quad x_2 = \rho^{-1} X_2, \quad x_3 = X_3. \tag{10}$$

The associated principal stretches are $\lambda_1 = \rho, \lambda_2 = \rho^{-1}, \lambda_3 = 1$ and the deformation gradient tensor has the form

$$\mathbf{F} = \operatorname{diag}(\rho, \rho^{-1}, 1). \tag{11}$$

In conjunction with (4) and (11), the traction boundary condition, $(7)_2$ gives

$$p = \mu^{(j)}\rho^{-2} \equiv p^{(j)}, \quad j = \text{I, II}. \tag{12}$$

Therefore

$$\mathbf{s} = \mu^{(j)} \begin{bmatrix} \rho - \rho^{-3} & 0 & 0 \\ 0 & 0 & 0 \\ 0 & 0 & 1-\rho^{-2} \end{bmatrix} \equiv \mathbf{s}^{(j)}, \quad j = \text{I, II}. \tag{13}$$

All other boundary conditions are automatically satisfied by the homogeneous deformation (10).

Let T be the total (compressive) *thrust* applied onto each of the surfaces $X_1 = \pm l_1$ and let $A^{(j)}$ be the original area of the surface taken by material j (j = I or II) so that $A^{(\text{I})} + A^{(\text{II})} = 4l_2 l_3$. It then follows from (13) that

$$T = -(\rho - \rho^{-3})(\mu^{(\text{I})} A^{(\text{I})} + \mu^{(\text{II})} A^{(\text{II})}). \tag{14}$$

Note that T is monotonically decreasing in ρ from $T = \infty$ when $\rho = 0$ to $T = -\infty$ when $\rho = \infty$, with $T = 0$ when $\rho = 1$. Hence (14) can be inverted to give stretch as a function of thrust: $\rho = \rho(T)$, with the compressive case $0 < \rho < 1$ corresponding to $T > 0$.

We now turn to examine the possibility of bifurcation away from any such state by solutions which involve an additional incremental deformation $\mathbf{u}$ superposed onto this homogeneous solution. Attention is restricted to buckling that takes place in the (X_1, X_2)-plane in the following plane strain fashion:

$$x_1 = \rho X_1 + \varepsilon u_1(X_1, X_2), \quad x_2 = \rho^{-1} X_2 + \varepsilon u_2(X_1, X_2), \quad x_3 = X_3, \tag{15}$$

where the unknown functions u_1 and u_2 are assumed to be independent of X_3 and ε is an order parameter which is used to obtain a linearized problem governing bifurcation from the homogeneous solution. If the pressure field and the associated Piola-Kirchoff stress tensor are given by

$$\begin{aligned} p(\mathbf{X}, \varepsilon) &= p^{(j)} + \varepsilon \bar{p}(X_1, X_2, X_3) + \mathrm{O}(\varepsilon^2), \\ \mathbf{s}(\mathbf{X}, \varepsilon) &= \mathbf{s}^{(j)} + \varepsilon \bar{\mathbf{s}}(X_1, X_2, X_3) + \mathrm{O}(\varepsilon^2), \end{aligned} \quad j = \text{I, II}, \tag{16}$$

respectively, then substituting from (15) into $(2)_2$ and (3) and retaining terms of order ε gives

$$\rho^{-2} u_{1,1} + u_{2,2} = 0, \tag{17}$$

while substituting from (15) into (4) and (5) and retaining terms of order ε gives

$$\operatorname{div} \bar{\mathbf{s}}^T = \mathbf{0}, \tag{18}$$

where

$$\bar{\mathbf{s}} = \begin{bmatrix} -\rho^{-1}\bar{p} + \mu^{(j)}(u_{1,1} - \rho^{-2} u_{2,2}) & \mu^{(j)}(u_{2,1} + \rho^{-2} u_{1,2}) & 0 \\ \mu^{(j)}(u_{1,2} + \rho^{-2} u_{2,1}) & -\rho\bar{p} + 2\mu^{(j)} u_{2,2} & 0 \\ 0 & 0 & -\bar{p} \end{bmatrix}. \tag{19}$$

Now $(18)_3$ is satisfied if $\bar{p}(X_1, X_2, X_3) = \bar{p}(X_1, X_2)$, thus giving that (17) and $(18)_{1,2}$ are three linear, homogeneous partial differential equations for $u_1(X_1, X_2)$, $u_2(X_1, X_2)$ and $\bar{p}(X_1, X_2)$. Turning now to examine the order ε boundary and interface conditions, one verifies that those obtained from (8) are automatically satisfied by virtue of $(15)_3$ and (19). Following Sawyers and Rivlin (1974), the following forms

$$u_1 = \begin{Bmatrix} -\sin(\Omega X_1) \\ \cos(\Omega X_1) \end{Bmatrix} U_1(X_2),$$

$$u_2 = \begin{Bmatrix} \cos(\Omega X_1) \\ \sin(\Omega X_1) \end{Bmatrix} U_2(X_2),$$

$$\tilde{p} = \begin{Bmatrix} \cos(\Omega X_1) \\ \sin(\Omega X_1) \end{Bmatrix} P(X_2), \tag{20}$$

are consistent with both (i) seperation of variables in the system of partial differential equations mentioned above, and (ii) the boundary conditions (6) provided that

$$\Omega = \frac{m\pi}{2l_1}, \quad m = \begin{cases} 2, 4, 6, 8 \ldots & \text{for the upper terms in (20),} \\ 1, 3, 5, 7 \ldots & \text{for the lower terms in (20).} \end{cases} \tag{21}$$

Under (20), the system of partial differential equations (17) and $(18)_{1,2}$ reduce to the single fourth order ordinary differential equation for $U_2(X_2)$:

$$U_2'''' - [1+\lambda^2]\Omega^2 U_2'' + \lambda^2 \Omega^4 U_2 = 0, \tag{22}$$

where the prime denotes differentiation with respect to X_2 and we have introduced a new stretch ratio

$$\lambda = \frac{\lambda_2}{\lambda_1} = \rho^{-2}. \tag{23}$$

The remaining two functions $U_1(X_2)$ and $P(X_2)$ are then given by

$$U_1(X_2) = \frac{1}{\lambda\Omega} U_2'(X_2),$$

$$P(X_2) = P^{(j)}(X_2) = \frac{\mu^{(j)}}{\lambda^{3/2}\Omega^2} \{U_2'''(X_2) - \Omega^2 U_2'(X_2)\}, \quad j = \text{I, II}. \tag{24}$$

The general solution of (22) is given by

$$U_2(X_2) = L_1(X_2)\cosh(\Omega X_2) + L_2(X_2)\sinh(\Omega X_2) + M_1(X_2)\cosh(\lambda\Omega X_2) + M_2(X_2)\sinh(\lambda\Omega X_2), \tag{25}$$

where $L_i(X_2)$ and $M_i(X_2)$, $i = 1, 2$, are constant in each ply. Thus $L_i(X_2)$ and $M_i(X_2)$ are step functions

$$L_i(X_2) = L_i^{(k)}, \quad M_i(X_2) = M_i^{(k)}, \quad i = 1, 2 \tag{26}$$

where $k = 1, \ldots, N$ refer to the in general different values of these constants in each of the N plies. There are thus $4N$ unknown constants to be determined, and it only remains to satisfy the $O(\varepsilon)$ boundary and interface conditions generated by (7) and (9). The condition on s_{23} in (7) is satisfied automatically, while the remaining conditions in (7) yield four relations binding the $4N$ unknown constants. Similarly the continuity of s_{23} and x_3 in (9) is satisfied automatically, while the remaining conditions in (9) yield $4(N-1)$ relations binding the $4N$ unknown constants. In total, this gives $4N$ relations, which are linear in the unknown constants, and so may be written as

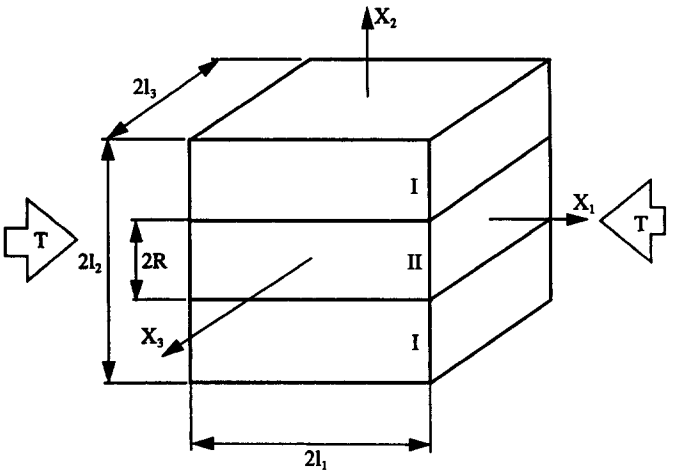

Fig. 1. The symmetric three-ply composite plate considered by Pence and Song (1991) and re-examined here for additional buckling solutions. Plane strain buckling takes place in the (X_1, X_2)-plane.

$$\mathbf{J}_{4N\times 4N}\mathbf{l}_{4N\times 1} = \mathbf{0}_{4N\times 1}, \tag{27}$$

where $\mathbf{l}$ is the vector containing the $4N$ unknowns in (26). The existence of nontrivial solutions for this system of equations requires that

$$\det \mathbf{J}_{4N\times 4N} = 0. \tag{28}$$

This is the basic bifurcation condition for the buckling problem of the N-ply neo-Hookean plate under thrust.

3. ADDITIONAL FAMILIES OF BUCKLED SOLUTIONS FOR THE SYMMETRIC THREE-PLY COMPOSITE PLATE

In this section we re-examine the bifurcation condition (28) for the symmetric three-ply plate ($N = 3$) as studied by Pence and Song (1991). Here $R_1 = R_2 = l_2$ where plies 1, 2 and 3 are, respectively, given by $-l_2 < X_2 < -R$, $-R < X_2 < R$, $R < X_2 < l_2$. If $\mu^{(1)}$ is the neo-Hookean shear modulus for ply-1 and ply-3, and $\mu^{(II)}$ is the neo-Hookean shear modulus for ply-2 as illustrated in Fig. 1, then (26) becomes

$$L_i(X_2) = \begin{bmatrix} L_i^{(1)} \\ L_i^{(2)} \\ L_i^{(3)} \end{bmatrix}, \quad M_i(X_2) = \begin{bmatrix} M_i^{(1)} & -l_2 \leqslant X_2 \leqslant -R \\ M_i^{(2)}, \quad i = 1,2, & -R \leqslant X_2 \leqslant R \\ M_i^{(3)} & R \leqslant X_2 \leqslant l_2 \end{bmatrix} \tag{29}$$

and the bifurcation condition (28) becomes $\det \mathbf{J}_{12\times 12} = 0$.

Now following Sawyers and Rivlin (1974), and Pence and Song (1991), attention is restricted to the two subclasses of *flexural buckling deformations* and *barrelling buckling deformations*, which exist as a consequence of the special symmetric nature of the three-ply composite construction presently under consideration. A flexural deformation is one in which $U_2(X_2)$ is an even function, whereupon (24) gives that $U_1(X_2)$ and $P(X_2)$ are each odd functions. This will be true provided that $(L_1^{(1)}, L_2^{(1)}, M_1^{(1)}, M_2^{(1)}) = (L_1^{(3)}, -L_2^{(3)}, M_1^{(3)}, -M_2^{(3)})$, $M_2^{(2)} = L_2^{(2)} = 0$. Thus a linear system remains for 6 independent constants, which are taken to be $\mathbf{l} = [L_1^{(1)}, L_2^{(1)}, M_1^{(1)}, M_2^{(1)}, L_1^{(2)}, M_1^{(2)}]^T$. The associated 6×6 coefficient matrix is given by

$$\mathbf{J}_F = \begin{bmatrix} \Lambda C_1 & -\Lambda S_1 & 2\lambda C_2 & -2\lambda S_2 & 0 & 0 \\ -2S_1 & 2C_1 & -\Lambda S_2 & \Lambda C_2 & 0 & 0 \\ -C_3 & S_3 & -C_4 & S_4 & C_3 & C_4 \\ S_3 & -C_3 & \lambda S_4 & -\lambda C_4 & -S_3 & -\lambda S_4 \\ -\Lambda C_3 & \Lambda S_3 & -2\lambda C_4 & 2\lambda S_4 & \Lambda\beta C_3 & 2\lambda\beta C_4 \\ 2S_3 & -2C_3 & \Lambda S_4 & -\Lambda C_4 & -2\beta S_3 & -\Lambda\beta S_4 \end{bmatrix}, \tag{30}$$

where

$$\begin{gathered} C_1 = \cosh(\eta), \quad C_2 = \cosh(\lambda\eta), \quad C_3 = \cosh(\eta\alpha), \quad C_4 = \cosh(\lambda\eta\alpha), \\ S_1 = \sinh(\eta), \quad S_2 = \sinh(\lambda\eta), \quad S_3 = \sinh(\eta\alpha), \quad S_4 = \sinh(\lambda\eta\alpha), \\ \Lambda = \lambda + 1/\lambda, \end{gathered} \tag{31}$$

and the parameters η, β and α are defined in (35) below. The associated flexural buckling equation is then written as

$$\Psi_F(\lambda, \eta, \beta, \alpha) \equiv \det \mathbf{J}_F = 0. \tag{32}$$

In contrast, a barrelling deformation is one in which $U_2(X_2)$ is an odd function. In a completely analogous fashion, the barrelling buckling equation is:

$$\Psi_B(\lambda, \eta, \beta, \alpha) \equiv \det \mathbf{J}_B = 0, \tag{33}$$

where $\mathbf{J}_B$ is the 6×6 matrix:

$$\mathbf{J}_B = \begin{bmatrix} \Lambda C_1 & -\Lambda S_1 & 2\lambda C_2 & -2\lambda S_2 & 0 & 0 \\ -2S_1 & 2C_1 & -\Lambda S_2 & \Lambda C_2 & 0 & 0 \\ -C_3 & S_3 & -C_4 & S_4 & -S_3 & -S_4 \\ S_3 & -C_3 & \lambda S_4 & -\lambda C_4 & C_3 & \lambda C_4 \\ -\Lambda C_3 & \Lambda S_3 & -2\lambda C_4 & 2\lambda S_4 & -\Lambda\beta S_3 & -2\lambda\beta S_4 \\ 2S_3 & -2C_3 & \Lambda S_4 & -\Lambda C_4 & 2\beta C_3 & \Lambda\beta C_4 \end{bmatrix}, \tag{34}$$

and the same notations (31) are used.The corresponding six constants for the barrelling deformation are $\mathbf{l} = [L_1^{(1)}, L_2^{(1)}, M_1^{(1)}, M_2^{(1)}, L_2^{(2)}, M_2^{(2)}]^T$. The eqns (32) and (33) relate the four dimensionless parameters:

$$\eta = \Omega l_2 = \frac{m\pi l_2}{2l_1}, \quad \beta = \frac{\mu^{(II)}}{\mu^{(I)}}, \quad \alpha = \frac{R}{l_2}, \quad \lambda = \frac{\lambda_2}{\lambda_1} = \rho^{-2}, \tag{35}$$

which are described as follows: (1) the *ripple parameter* η scales the discrete ripple number m with respect to the aspect ratio l_2/l_1, this parameter is often treated in the analysis as a continuous variable; (2) the *stiffness ratio* β is the ratio of the shear modulus of material-II to that of material-I; (3) the *volume fraction* α is the ratio of the thickness of the central ply to the thickness of the whole composite plate; and (4) λ is the ratio of principal stretches, which in view of (14) and (23) is the *load parameter* with $\lambda = 1$ corresponding to no load and λ monotonically increasing from $\lambda = 1$ as the compressive thrust T increases. Their respective ranges are

$$\eta > 0, \quad \beta > 0, \quad 0 \leqslant \alpha \leqslant 1, \quad \lambda > 0. \tag{36}$$

A pair of material parameters (β, α), together with l_1, l_2 and l_3 specifies a specific symmetric three-ply construction. Each of the special values

$$\beta = 1 \quad \text{or} \quad \alpha = 0 \quad \text{or} \quad \alpha = 1 \tag{37}$$

correspond to the special case of a noncomposite plate, conversely values of the pair (β, α) obeying $(36)_{2,3}$ with $\beta \neq 1$ and $\alpha \neq 0$ and $\alpha \neq 1$ are associated with *genuinely composite* constructions. The pair (β, α) constitute the *composite characterization parameters* mentioned previously in the Introduction. It is to be noted in all cases that the absence of load $(\lambda = 1)$ trivially furnishes a solution to both (32) and (33) in view of the coalescence of the final two columns of $\mathbf{J}_F$ and $\mathbf{J}_B$.

Pence and Song (1991) investigated solutions of both (32) and (33) by fixing (η, β, α) obeying $(36)_{1,2,3}$ and showing numerically that each of these equations then admits a solution λ obeying $\lambda > 1$ and hence corresponding to compression. These solutions, denoted by $\lambda = \Phi_F(\eta, \beta, \alpha)$ for (32) and $\lambda = \Phi_B(\eta, \beta, \alpha)$ for (33) were determined numerically by means of a searching and bisection algorithm and in each case resulted in the minimum value of $\lambda > 1$ compatible with (32) or (33) for the given (η, β, α). For fixed (β, α), each of these λ-values were found to approach a common asymptotic value $\lambda_\infty = \lambda_\infty(\beta, \alpha)$ as $\eta \to \infty$; this value was then computed numerically by taking a large cut-off value of η. *Left unaddressed in Pence and Song* (1991) *is the possibility of additional roots* λ *greater than those given by* $\Phi_F(\eta, \beta, \alpha)$ *and* $\Phi_B(\eta, \beta, \alpha)$, *as well as the possibility that the asymptotic values* λ_∞ *associated with wrinkling can be computed by analytical means.* This section deals with the further investigation of these two issues. The first issue leads us to analyze (32) and (33) for large λ, and the second leads us to analyse (32) and (33) for large η.

When the matrix $\mathbf{J}_F$ in (30) is compared with the matrix $\mathbf{J}_B$ in (34), the only difference is in the last two columns of each matrix. In fact, $\Psi_F(\lambda, \eta, \beta, \alpha)$ may be transformed into $\Psi_B(\lambda, \eta, \beta, \alpha)$ by exchanging η and $\lambda\eta$ in the hyperbolic trigonometric functions of (31), i.e.

$$\{\Psi_F(\lambda, \eta, \beta, \alpha) \leftrightarrow \Psi_B(\lambda, \eta, \beta, \alpha)\} \Leftrightarrow \begin{Bmatrix} C_1 \leftrightarrow C_2, & S_1 \leftrightarrow S_2 \\ C_3 \leftrightarrow C_4, & S_3 \leftrightarrow S_4 \end{Bmatrix}. \tag{38}$$

This claim may be verified by first subjecting (30) to the exchanges on the right hand side of the $\Leftrightarrow$ in (38), and then performing the following row operations: exchange column 1 with column 4, exchange column 2 with column 3, exchange column 5 with column 6, exchange row 1 with row 2, exchange row 3 with row 4, exchange row 5 with row 6, multiply rows 1, 4, and 5 by λ, and finally, multiply columns 1, 2, and 5 by λ^{-1}. Under this set of operations Ψ_F is transformed into Ψ_B. Relations (38) will enable us to analyse many aspects of the flexural and barrelling cases in a common setting. To this end it will be useful to introduce the subscript $*$ as a placeholder for either the subscript F for flexural deformation or the subscript B for the barrelling deformation.

The expressions Ψ_F and Ψ_B given in (32) and (33) may be expanded into the following sum of products of hyperbolic functions and polynomials:

$$\Psi_*(\lambda, \eta, \beta, \alpha) = \frac{1}{8}\mathbf{H}_*\mathbf{P}\Lambda, \tag{39}$$

where

$$\mathbf{H}_* = \mathbf{H}_*(\lambda, \eta, \alpha)_{1\times 10} = \{\sinh(\eta\kappa_1), \sinh(\eta\kappa_2), \ldots, \sinh(\eta\kappa_{10})\}, \tag{40}$$

$$\mathbf{P} = [P_{i,j}(\beta)]_{10\times 10}, \tag{41}$$

$$\Lambda = \Lambda(\lambda)_{10\times 1} = \{\lambda^{-4}, \lambda^{-3}, \ldots, \lambda^0, \ldots, \lambda^4, \lambda^5\}^T. \tag{42}$$

In equation (39), the only difference between the flexural and barrelling case are the values for $\kappa_i = \kappa_i(\lambda, \alpha)$ $(i = 1, \ldots, 10)$ in (40). These values, as well as the elements of the matrix $\mathbf{P}$, are given in Appendix A. It is to be noted that $\mathbf{H}_*(\lambda, 0, \alpha) = \mathbf{0}$, so that (39) gives $\Psi_*(\lambda, 0, \beta, \alpha) \equiv 0$.

We now conduct an analysis of $\Psi_*(\lambda, \eta, \beta, \alpha)$, in (39), for large λ in order to gain insight as to the total number of roots λ to (32) and (33) for fixed (η, β, α). For large λ the leading order terms in (39) will be those containing both λ^5 from (42) and $e^{\eta(\lambda+1)}$, $e^{\eta(\lambda-1)}$, $e^{\eta(\lambda+2\alpha-1)}$ and $e^{\eta(\lambda-2\alpha+1)}$ from (40) [*viz.* (A.5) and (A.6)]. It follows that, for the flexural deformation,

$$\Psi_F(\lambda, \eta, \beta, \alpha) \sim \frac{\lambda^5}{16}(\beta-1)^2 e^{\eta\lambda}[e^{\eta} - e^{-\eta} - e^{\eta(2\alpha-1)} + e^{-\eta(2\alpha-1)}], \tag{43}$$

provided that both $\beta \neq 1$ and $\alpha \neq 1$; and for the barrelling deformation,

$$\Psi_B(\lambda, \eta, \beta, \alpha) \sim \frac{\lambda^5}{16}(\beta-1)^2 e^{\eta\lambda}[e^{\eta} + e^{-\eta} - e^{\eta(2\alpha-1)} - e^{-\eta(2\alpha-1)}], \tag{44}$$

provided that $\beta \neq 1$, $\alpha \neq 1$ and $\alpha \neq 0$. Hence (43) and (44) give

$$\Psi_*(\lambda, \eta, \beta, \alpha) \sim \omega_*(\eta, \beta, \alpha) e^{\eta\lambda}\lambda^5 \tag{45}$$

where

$$\omega_F(\eta, \beta, \alpha) = \frac{1}{4}(\beta-1)^2 \cosh(\eta\alpha) \sinh[\eta(1-\alpha)], \tag{46}$$

$$\omega_B(\eta, \beta, \alpha) = \frac{1}{4}(\beta-1)^2 \sinh(\eta\alpha) \sinh[\eta(1-\alpha)], \tag{47}$$

for the flexural deformation and the barrelling deformation, respectively. For genuinely composite constructions ($\beta \neq 1$, $\alpha \neq 1$, and $\alpha \neq 0$) the expression $\omega_*(\eta, \beta, \alpha) e^{\eta\lambda}\lambda^5$ does not vanish and as such is a convenient normalization for $\Psi_*(\lambda, \eta, \beta, \alpha)$. Let

$$\Pi_*(\lambda, \eta, \beta, \alpha) \equiv \frac{\Psi_*(\lambda, \eta, \beta, \alpha)}{\omega_*(\eta, \beta, \alpha) e^{\eta\lambda}\lambda^5}, \tag{48}$$

so that, in a genuinely composite construction, the buckling equations (32) and (33) are equivalent to

$$\Pi_*(\lambda, \eta, \beta, \alpha) = 0, \tag{49}$$

with $* = F$ and $* = B$, respectively, and $\Pi_*(\lambda, \eta, \beta, \alpha) \to 1$ as $\lambda \to \infty$. We have numerically studied the functions $\Pi_*(\lambda, \eta, \beta, \alpha)$ for fixed (η, β, α) in genuinely composite constructions and found that both $* = F$ and $* = B$ will in general each yield two roots $\lambda > 1$ for (49) before $\Pi_*(\lambda, \eta, \beta, \alpha)$ begins to smoothly approach its asymptotic value of one. This is

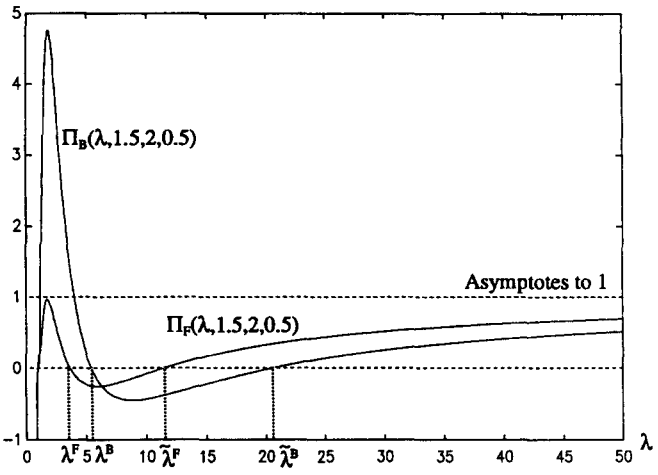

Fig. 2. The functions $\Pi_F(\lambda, \eta, \beta, \alpha)$ and $\Pi_B(\lambda, \eta, \beta, \alpha)$ defined in (48) for the case $\eta = 1.5$, $\beta = 2$, $\alpha = 0.5$. Each of these functions has two roots λ in the range $\lambda > 1$, and each function approaches the asymptotic value one as $\lambda \to \infty$.

demonstrated in Fig. 2 for the case $(\eta, \beta, \alpha) = (1.5, 2.0, 0.5)$ which exhibits the ever present root $\lambda = 1$ and the smooth approach to the asymptotic value of 1 for both $\Pi_F(\lambda, 1.5, 2.0, 0.5)$ and $\Pi_B(\lambda, 1.5, 2.0, 0.5)$. For $1 < \lambda < \infty$, this figure indicates the presence of two roots λ to the equation $\Pi_F(\lambda, 1.5, 2.0, 0.5) = 0$, the first of which is given by $\lambda^F \approx 3.67$ and the second of which is given by $\tilde{\lambda}^F \approx 11.46$. Similarly, the equation $\Pi_B(\lambda, 1.5, 2.0, 0.5) = 0$ has two roots λ given by $\lambda^B \approx 5.45$ and $\tilde{\lambda}^B \approx 20.53$. A similar situation prevails for all other values (η, β, α) associated with genuinely composite construction, namely there exist roots λ^F and $\tilde{\lambda}^F$ for (49) whenever $* = F$, and there exist roots λ^B and $\tilde{\lambda}^B$ for (49) whenever $* = B$, with these roots obeying

$$1 < \lambda^F < \tilde{\lambda}^F, \quad 1 < \lambda^B < \tilde{\lambda}^B. \tag{50}$$

The functions taking (η, β, α) to these four roots will be denoted by $\Phi_F(\eta, \beta, \alpha)$, $\tilde{\Phi}_F(\eta, \beta, \alpha)$, $\Phi_B(\eta, \beta, \alpha)$ and $\tilde{\Phi}_B(\eta, \beta, \alpha)$. The roots λ^F and λ^B and the functions $\Phi_F(\eta, \beta, \alpha)$ and $\Phi_B(\eta, \beta, \alpha)$ were obtained previously in Pence and Song (1991). The study of Pence and Song (1991) however did not uncover the additional roots $\tilde{\lambda}^F$ and $\tilde{\lambda}^B$ owing to numerical instabilities connected with seeking roots λ to (32) and (33) whenever λ is larger than the respective first roots λ^F and λ^B. The scaling (48) suggested by the large λ asymptotic analysis overcomes this difficulty and thus enables us to uncover the new roots $\tilde{\lambda}^F$ and $\tilde{\lambda}^B$. These two new roots are each associated with a new family of buckled configurations for the symmetric three-ply construction. The subsequent numerical approach of $\Pi_* \to 1$ as $\lambda \to \infty$ strongly suggests that all roots to (32) and (33) are now accounted for.

Numerical study of the four functions $\Phi_F(\eta, \beta, \alpha)$, $\tilde{\Phi}_F(\eta, \beta, \alpha)$, $\Phi_B(\eta, \beta, \alpha)$ and $\tilde{\Phi}_B(\eta, \beta, \alpha)$ indicates that each of these functions varies smoothly with (η, β, α) and obeys the ordering relation

$$1 < \Phi_F(\eta, \beta, \alpha) < \Phi_B(\eta, \beta, \alpha) < \tilde{\Phi}_F(\eta, \beta, \alpha) < \tilde{\Phi}_B(\eta, \beta, \alpha). \tag{51}$$

Furthermore, for fixed (β, α) corresponding to a genuinely composite construction, we find as $\eta \to 0$ that

$$\lim_{\eta \to 0} \Phi_F(\eta, \beta, \alpha) = 1,$$

$$\lim_{\eta \to 0} \Phi_B(\eta, \beta, \alpha) = \lim_{\eta \to 0} \tilde{\Phi}_F(\eta, \beta, \alpha) = \lim_{\eta \to 0} \tilde{\Phi}_B(\eta, \beta, \alpha) = \infty. \tag{52}$$

Moreover, as $\eta \to \infty$, we find that

$$\lim_{\eta\to\infty} \Phi_F(\eta, \beta, \alpha) = \lim_{\eta\to\infty} \Phi_B(\eta, \beta, \alpha) = \lambda_\infty(\beta, \alpha),$$
$$\lim_{\eta\to\infty} \tilde{\Phi}_F(\eta, \beta, \alpha) = \lim_{\eta\to\infty} \tilde{\Phi}_B(\eta, \beta, \alpha) = \tilde{\lambda}_\infty(\beta, \alpha), \tag{53}$$

where $\lambda_\infty(\beta, \alpha) < \tilde{\lambda}_\infty(\beta, \alpha)$. Equations (51)–(53) are in accordance with the results given in Pence and Song (1991) for the functions $\Phi_F(\eta, \beta, \alpha)$, $\Phi_B(\eta, \beta, \alpha)$ and $\lambda_\infty(\beta, \alpha)$, and extend these results to encompass the new functions $\tilde{\Phi}_F(\eta, \beta, \alpha)$, $\tilde{\Phi}_B(\eta, \beta, \alpha)$ and $\tilde{\lambda}_\infty(\beta, \alpha)$ associated with the new buckled configurations uncovered in the present extended study.

The functions $\Phi_F(\eta, \beta, \alpha)$, $\tilde{\Phi}_F(\eta, \beta, \alpha)$, $\Phi_B(\eta, \beta, \alpha)$ and $\tilde{\Phi}_B(\eta, \beta, \alpha)$ determine four families of failure stretch ratios:

$$\lambda_m^F = \Phi_F(m\pi l_2/2l_1, \beta, \alpha),$$
$$\lambda_m^B = \Phi_B(m\pi l_2/2l_1, \beta, \alpha),$$
$$\tilde{\lambda}_m^F = \tilde{\Phi}_F(m\pi l_2/2l_1, \beta, \alpha),$$
$$\tilde{\lambda}_m^B = \tilde{\Phi}_B(m\pi l_2/2l_1, \beta, \alpha), \quad m = 1, 2, 3\ldots \tag{54}$$

owing to the discrete nature of η as given in $(35)_1$. The corresponding four families of failure thrusts: T_m^F, T_m^B, $\tilde{T}_m^F$, and $\tilde{T}_m^B$, $m = 1, 2, 3\ldots$ are then obtained from (14) upon using $\rho = \lambda^{-1/2}$. These failure thrusts are ordered the same as the failure stretch ratios. In the event that $\Phi_F(\eta, \beta, \alpha)$ is monotonically increasing in η to $\lambda_\infty(\beta, \alpha)$ and $\Phi_B(\eta, \beta, \alpha)$ is monotonically decreasing in η to $\lambda_\infty(\beta, \alpha)$, then

$$0 < T_1^F < T_2^F < \cdots < T_m^F < T_{m+1}^F < \cdots < T_\infty < \cdots < T_{m+1}^B < T_m^B < \cdots < T_2^B < T_1^B, \tag{55}$$

where T_∞ is a wrinkling thrust associated with the stretch ratio $\lambda_\infty(\beta, \alpha)$. In particular, as established by Sawyers and Rivlin (1974), this occurs for the noncomposite case (37); the corresponding curves $\Phi_F(\eta, \beta, \alpha)$ and $\Phi_B(\eta, \beta, \alpha)$ are displayed in Fig. 3. As shown in Pence and Song (1991) certain pairs (β, α) are associated with a loss of monotonicity in $\Phi_B(\eta, \beta, \alpha)$

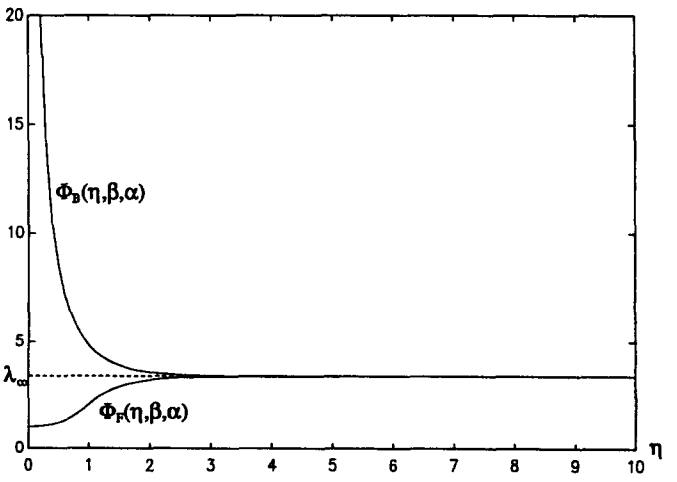

Fig. 3. The functions $\Phi_F(\eta, \beta, \alpha)$ and $\Phi_B(\eta, \beta, \alpha)$ for parameter pairs (β, α) corresponding to the noncomposite case as given in (37)

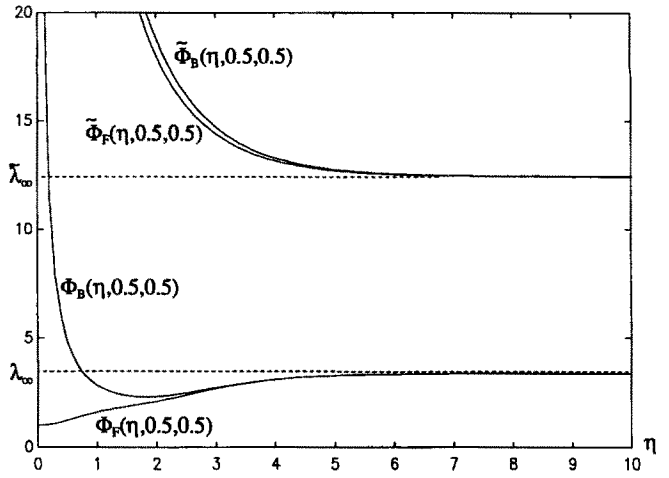

Fig. 4. The functions $\Phi_F(\eta, \beta, \alpha)$, $\Phi_B(\eta, \beta, \alpha)$, $\tilde{\Phi}_F(\eta, \beta, \alpha)$ and $\tilde{\Phi}_B(\eta, \beta, \alpha)$ for $\beta = 0.5$, $\alpha = 0.5$. The two lower curves were displayed previously in Fig. 4 of Pence and Song (1991). The two upper curves correspond to the new families of buckled solutions.

as a function of ripple parameter η. Figure 4 depicts one such example for the pair $(\beta, \alpha) = (0.5, 0.5)$. Furthermore, certain pairs (β, α) are also associated with a loss of monotonicity in $\Phi_F(\eta, \beta, \alpha)$ as a function of η. Figure 5 depicts one such example for the pair $(\beta, \alpha) = (2.0, 0.5)$. In such cases the possibility arises that the failure thrusts T_m^F, and T_m^B, will no longer obey (55), but instead will be interlaced. In all cases (51) ensures that the lowest, or critical, thrust will be one of the T_m^F for some positive integer m including, possibly, $m = \infty$. If $\Phi_F(\eta, \beta, \alpha)$ is monotonically increasing to λ_∞ then this critical thrust will be T_1^F, however if $\Phi_F(\eta, \beta, \alpha)$ is not monotonic, then this critical thrust may occur for $m \neq 1$ and indeed may be associated with the wrinkling thrust $T_\infty^F = T_\infty$. A detailed study of such phenomena as they occur among the two families T_m^F, and T_m^B, $(m = 1, 2, \ldots)$, with particular emphasis on their correlation to parameter pairs (β, α) and aspect ratio l_2/l_1 is given in Pence and Song (1991).

We thus turn our attention to the two new families of failure thrusts $\tilde{T}_m^F$ and $\tilde{T}_m^B$ $(m = 1, 2, \ldots)$. Consider first the case in which both $\tilde{\Phi}_F(\eta, \beta, \alpha)$ and $\tilde{\Phi}_B(\eta, \beta, \alpha)$ are monotonically decreasing toward the asymptote $\tilde{\lambda}_\infty(\beta, \alpha)$ as for example occurs in Fig. 4. Then $\tilde{T}_1^B$ is the maximum thrust from among these two families, and $\tilde{T}_\infty$ is the minimum thrust,

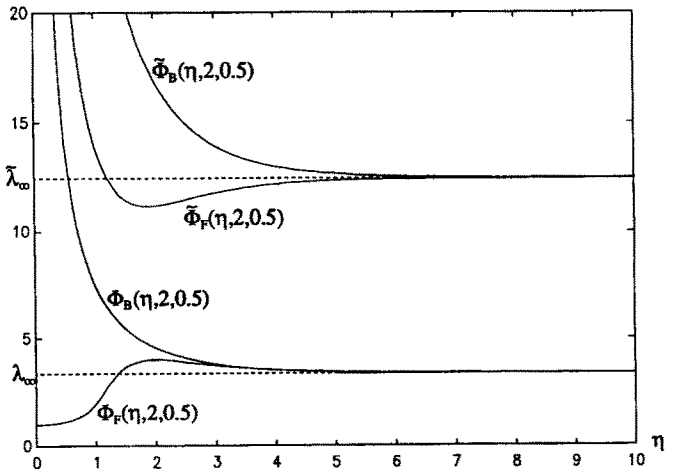

Fig. 5. The functions $\Phi_F(\eta, \beta, \alpha)$, $\Phi_B(\eta, \beta, \alpha)$, $\tilde{\Phi}_F(\eta, \beta, \alpha)$ and $\tilde{\Phi}_B(\eta, \beta, \alpha)$ for $\beta = 2$, $\alpha = 0.5$. The two lower curves were displayed previously in Fig. 5 of Pence and Song (1991), while the two upper curves correspond to the new families of buckled solutions.

where $\tilde{T}_\infty$ is the newly uncovered wrinkling thrust associated with $\tilde{\lambda}_\infty$. The remaining thrusts will lie between these values, and the two families of thrusts will interlace their values. However for fixed ripple number m, (51) ensures that $\tilde{T}_m^F < \tilde{T}_m^B$. The question arises as to whether or not the thrusts from these two new families can interlace themselves with the thrusts from the two original families. For the case depicted in Fig. 4, no interlacing can occur with the original flexure family, since the interval $\lambda_\infty < \lambda < \tilde{\lambda}_\infty$ isolates the range of the curve $\Phi_F(\eta, \beta, \alpha)$ from the range of the curves $\tilde{\Phi}_F(\eta, \beta, \alpha)$ and $\tilde{\Phi}_B(\eta, \beta, \alpha)$. However no such isolation occurs between the latter two ranges and that of $\Phi_B(\eta, \beta, \alpha)$ since $\Phi_B(\eta, \beta, \alpha) \to \infty$ as $\eta \to 0$. Thus if the separation between the discrete η values is sufficiently small, some of the low ripple number thrusts of the original barrelling family will be interlaced with some of the higher ripple number thrusts of the two new families. The separation between discrete η values is determined by the aspect ratio l_2/l_1, thus for fixed plate height l_2, this interlacing will occur if the plate length in the direction of thrust l_1 is sufficiently large.

Symmetric three-ply plates corresponding to other pairs (β, α) give rise to fairly similar phenomena, with the departure from the behavior described above determined by the extent to which the functions $\tilde{\Phi}_F(\eta, \beta, \alpha)$ and $\tilde{\Phi}_B(\eta, \beta, \alpha)$ are not monotonic in η. For example in the case $(\beta, \alpha) = (2.0, 0.5)$ depicted in Fig. 5, the curve $\tilde{\Phi}_F(\eta, \beta, \alpha)$ exhibits a local minimum. Thus in this case $\tilde{T}_\infty$ is not the minimum failure thrust from among the two new families. Instead this minimum failure thrust will occur at some finite ripple number m within the new flexure thrust family $\tilde{T}_m^F$.

The ordering possibilities for the new thrusts $\tilde{T}_m^F$ and $\tilde{T}_m^B$ could certainly be characterized in a systematic fashion by utilizing a methodology similar to that developed in Pence and Song (1991) for the previously known thrusts T_m^F and T_m^B. However, since (51) ensures in all cases that the critical failure thrust remains associated with the original flexure family T_m^F, such a detailed study will not be pursued. In addition, we note that the conclusions of the optimal design study given in Song and Pence (1992) are not affected by the existence of the two new families $\tilde{T}_m^F$ and $\tilde{T}_m^B$ of buckling thrusts.

We now turn to an asymptotic analysis of the curves $\Phi_F(\eta, \beta, \alpha)$, $\tilde{\Phi}_F(\eta, \beta, \alpha)$, $\Phi_B(\eta, \beta, \alpha)$ and $\tilde{\Phi}_B(\eta, \beta, \alpha)$ as $\eta \to \infty$. This will yield an analytical characterization of the asymptotic values $\lambda_\infty(\beta, \alpha)$ and $\tilde{\lambda}_\infty(\beta, \alpha)$ associated with wrinkling, and will also clarify the apparent disappearance of the two new families of buckled solutions for the noncomposite case given by (37). Now (40) and (41), with (A.5) and (A.6), give

$$\kappa_1 = \max(\kappa_1, \kappa_2, \ldots, \kappa_9, \kappa_{10}) = \lambda + 1, \tag{56}$$

for both flexural and barrelling deformations. Hence

$$\Psi_*(\lambda, \eta, \beta, \alpha) \sim e^{\eta\kappa_1} P_1(\lambda, \beta), \quad \text{as } \eta \to \infty, \tag{57}$$

where

$$P_1(\lambda, \beta) \equiv \sum_{j=-4}^{5} P_{1,j}(\beta)\lambda^j, \tag{58}$$

and the polynomials $P_{1,j}(\beta)$ are given in Table A.1. Since the exponential function is always positive, (57) indicates that solutions of

$$P_1(\lambda, \beta) = 0 \tag{59}$$

yield asymptotic solutions to the buckling equations $\Psi_* = 0$ as $\eta \to \infty$. In particular, the wrinkling load parameters $\lambda_\infty(\beta, \alpha)$ and $\tilde{\lambda}_\infty(\beta, \alpha)$ must be roots of (59). We observe that, according to (59), these wrinkling load parameters are independent of the volume fraction α. Evaluating (58) with the aid of Table A.1 gives

$$P_1(\lambda, \beta) = \frac{1}{\lambda^4}(\lambda-1)^3 f_1(\lambda) f_2(\lambda, \beta), \tag{60}$$

where

$$f_1(\lambda) = (\lambda^3 - 3\lambda^2 - \lambda - 1), \tag{61}$$

$$f_2(\lambda, \beta) = (\beta-1)^2\lambda^3 - [3(\beta-1)^2+4\beta]\lambda^2 - [(\beta-1)^2+8\beta]\lambda - (\beta+1)^2. \tag{62}$$

The equation $f_1(\lambda) = 0$ has one real root λ_∞ given by Cardano's solution for the cubic polynomial equation,

$$\lambda_\infty = 1 + \sqrt[3]{2+\sqrt{4-(4/3)^3}} + \sqrt[3]{2-\sqrt{4-(4/3)^3}} = 3.38297577\ldots. \tag{63}$$

For $\beta \neq 1$ and $\beta \geq 0$, the equation $f_2(\lambda, \beta) = 0$ also yields exactly one real *positive* root, $\tilde{\lambda}_\infty(\beta)$. In fact, we find that the constant λ_∞ given in (63) is the asymptotic value $\lambda_\infty(\beta, \alpha)$ of $(53)_1$, and we also find that the root $\tilde{\lambda}_\infty(\beta)$ to $f_2(\lambda, \beta) = 0$ is the asymptotic value $\tilde{\lambda}_\infty(\beta, \alpha)$ given in $(53)_2$. Hence (53) can be improved to yield

$$\begin{aligned} &\lim_{\eta\to\infty} \Phi_F(\eta, \beta, \alpha) = \lim_{\eta\to\infty} \Phi_B(\eta, \beta, \alpha) = \lambda_\infty \approx 3.383, \\ &\lim_{\eta\to\infty} \tilde{\Phi}_F(\eta, \beta, \alpha) = \lim_{\eta\to\infty} \tilde{\Phi}_B(\eta, \beta, \alpha) = \tilde{\lambda}_\infty(\beta), \quad f_2(\tilde{\lambda}_\infty(\beta), \beta) = 0. \end{aligned} \tag{64}$$

In particular, $(64)_1$ is a significant improvement over the numerical cut-off procedure used for computing the wrinkling load parameter λ_∞ for the examples presented in Pence and Song (1991). Specifically, it is to be noted that some of the examples presented in Pence and Song (1991) were more successful than others in accurately attaining this constant asymptotic value $\lambda_\infty \approx 3.383$.

The dependence of $\tilde{\lambda}_\infty$ on β is depicted in Fig. 6, where it is to be noted that

$$\lim_{\beta\to 0} \tilde{\lambda}_\infty(\beta) = \lambda_\infty, \quad \lim_{\beta\to 1} \tilde{\lambda}_\infty(\beta) = \infty, \quad \lim_{\beta\to\infty} \tilde{\lambda}_\infty(\beta) = \lambda_\infty. \tag{65}$$

Here $(65)_1$ and $(65)_3$ follow from (62) since $f_2(\lambda, 0) = f_1(\lambda)$ and $f_2(\lambda, \beta) = \beta^2 f_1(\lambda) + O(\beta)$ as $\beta \to \infty$, whereas $(65)_2$ is a consequence of the observation that $f_2(\lambda, 1) = -4(\lambda+1)^2$ has no roots for positive λ. Since $\beta = 1$ corresponds to the case of noncomposite construction, $(65)_2$ leads one to anticipate that the two new families of failure thrusts $\tilde{T}_m^F$ and $\tilde{T}_m^B$, which

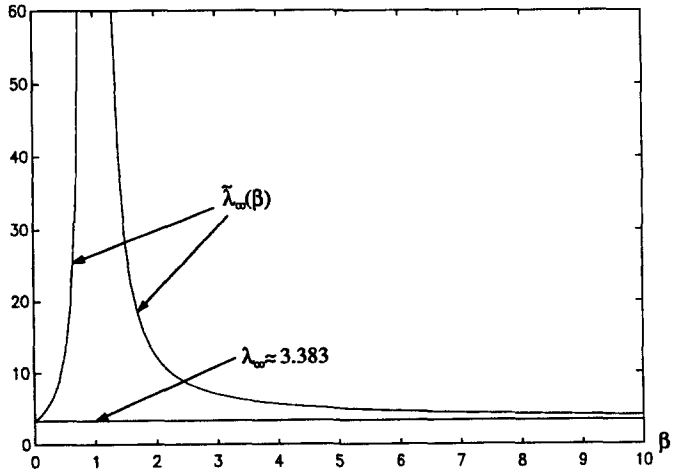

Fig. 6. The values of the wrinkling load parameters λ_∞ and $\tilde{\lambda}_\infty(\beta)$ which are the roots of (61) and (62) respectively. Here $\lambda_\infty = 3.38297\ldots$ and $\tilde{\lambda}_\infty(\beta)$ depends only on β. As $\beta \to 1$, corresponding to a noncomposite plate, $\tilde{\lambda}_\infty(\beta) \to \infty$.

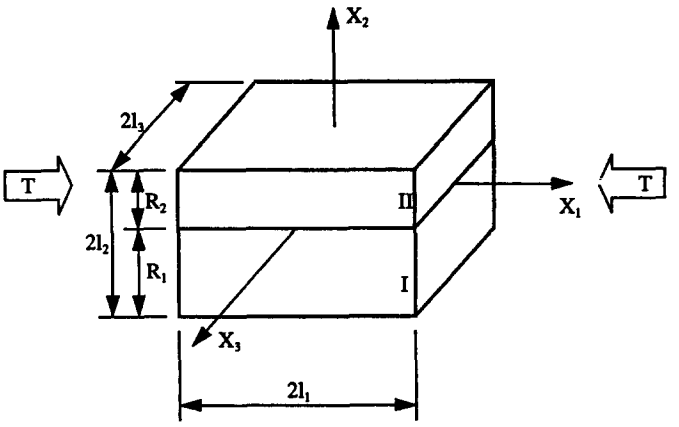

Fig. 7. The two-ply composite plate. Once again plane strain buckling is assumed to occur in the (X_1, X_2)-plane.

only exist for the genuinely composite construction, will individually retreat to infinity if the (β, α) parameter pair is made to approach any of the values (37) associated with noncomposite construction.

4. FAMILIES OF BUCKLED SOLUTIONS FOR THE TWO-PLY PLATE

It was shown in Pence and Song (1991) that the failure thrusts given in Sawyers and Rivlin (1974) for noncomposite construction, will reorder themselves for certain composite constructions. The results of the previous section indicate that, in addition, composite construction will also give rise to completely new families of failure thrusts. Specifically, the *symmetric three-ply* construction gives rise to two new families of failure thrusts as given by $(54)_3$ and $(54)_4$. The question thus arises as to how such new families will correlate with the total number of plies N in a more general construction. We here consider this question for the case of a two-ply construction as shown in Fig. 7. By setting the origin of the coordinate system at the interface between the two plies, then ply-1 occupies $-R_1 \leqslant X_2 \leqslant 0$ and ply-2 occupies $0 \leqslant X_2 \leqslant R_2$. The lack of symmetry in this problem does not allow the type of simplifications as given in Section 3 in which the 12×12 system for the symmetric three-ply problem reduced to two separate 6×6 systems [(32) and (33)] for flexural and barrelling bifurcations. Instead, for the two-ply problem, one must treat the full 8×8 system [(28) with $N = 2$] and the resulting buckled states will neither have the symmetry associated with flexure nor that associated with barrelling. One finds that if the eight constants in (26) are arranged as follows

$$\mathbf{l} = \{L_1^{(1)}, L_2^{(1)}, M_1^{(1)}, M_2^{(1)}, L_1^{(2)}, L_2^{(2)}, M_1^{(2)}, M_2^{(2)}\}^T, \tag{66}$$

then the coefficient matrix $\mathbf{J}$ of (27) is given by

$$\mathbf{J} = \begin{bmatrix} \Lambda C_3 & -\Lambda S_3 & 2\lambda C_4 & -2\lambda S_4 & 0 & 0 & 0 & 0 \\ -2S_3 & 2C_3 & -\Lambda S_4 & \Lambda C_4 & 0 & 0 & 0 & 0 \\ 1 & 0 & 1 & 0 & -1 & 0 & -1 & 0 \\ 0 & 1 & 0 & \lambda & 0 & -1 & 0 & -\lambda \\ -\Lambda & 0 & -2\lambda & 0 & \beta\Lambda & 0 & 2\beta\lambda & 0 \\ 0 & -2 & 0 & -\Lambda & 0 & 2\beta & 0 & \beta\Lambda \\ 0 & 0 & 0 & 0 & \Lambda C_5 & \Lambda S_5 & 2\lambda C_6 & 2\lambda S_6 \\ 0 & 0 & 0 & 0 & 2S_5 & 2C_5 & \Lambda S_6 & \Lambda C_6 \end{bmatrix}, \tag{67}$$

where C_3, C_4, S_3, S_4 and Λ are again given by (31) and

$$C_5 = \cosh(\eta(1-\alpha)), \quad C_6 = \cosh(\lambda\eta(1-\alpha)),$$
$$S_5 = \sinh(\eta(1-\alpha)), \quad S_6 = \sinh(\lambda\eta(1-\alpha)). \tag{68}$$

Thus, once again, four nondimensional parameters η, β, α and λ enter into $\mathbf{J}$. Here the stiffness ratio β and the load parameter λ are again given by $(35)_2$ and $(35)_4$, however the ripple parameter η and the volume fraction α are now no longer given by $(35)_1$ and $(32)_3$ but are instead given by

$$\eta = 2\Omega l_2 = \frac{m\pi l_2}{l_1}, \quad \alpha = \frac{R_1}{2l_2}. \tag{69}$$

Even so, the parameter ranges (36) remain in force. It is to be noted that interchanging the ply ordering results in (α, β) being transformed into $(1-\alpha, 1/\beta)$. Once again, if the material parameters (α, β) take the values in (37), then the two-ply problem considered here reduces to the noncomposite construction as studied by Sawyers and Rivlin (1974, 1982). In addition, as before, genuinely composite constructions obey $\beta \neq 1$, $\alpha \neq 0$ and $\alpha \neq 1$.

The necessary and sufficient condition for bifurcation to take place in the two-ply construction shall be written as

$$\Psi(\lambda, \eta, \beta, \alpha) \equiv \det \mathbf{J} = 0. \tag{70}$$

The analysis of (70) bears many similarities to the analysis of either (32) or (33). It is to be noted, however, that the size difference of the coefficient matrix $\mathbf{J}$ (64 entries) as compared to either $\mathbf{J}_F$ or $\mathbf{J}_B$ (36 entries each) serves to complicate the ensuring analysis. In view of the fairly detailed exposition given in the previous section, we shall here summarize the results of the analysis of (70) and refer the reader to Qiu (1992) for additional details. Once again the no-load case $\lambda = 1$ always furnishes a solution to (70) as then the first and third column of $\mathbf{J}$ are identical. A large λ expansion of $\mathbf{J}$ can be shown to yield

$$\Psi(\lambda, \eta, \beta, \alpha) = \omega(\eta, \beta, \alpha)\, e^{\eta\lambda}\lambda^7 + o(e^{\eta\lambda}\lambda^7), \tag{71}$$

for genuinely composite constructions where

$$\omega(\eta, \beta, \alpha) = \tfrac{1}{4}(1-\beta)^2 \sinh(\eta\alpha) \sinh[\eta(1-\alpha)] \neq 0, \tag{72}$$

which we note in fact coincides with the functional form given in (47). Thus we normalize the bifurcation equation (70) so as to give

$$\Pi(\lambda, \eta, \beta, \alpha) = \frac{\Psi(\lambda, \eta, \beta, \alpha)}{\omega(\eta, \beta, \alpha)\, e^{\eta\lambda}\lambda^7} = 0. \tag{73}$$

For fixed (η, β, α) corresponding to genuinely composite constructions, numerical evaluation of (73) reveals the existence of three roots λ obeying $\lambda > 1$ and also confirm that $\Pi(\lambda, \eta, \beta, \alpha) \to 1$ as $\lambda \to \infty$ (Fig. 8) so as to provide confidence that all possible roots are accounted for. These three roots shall be denoted by

$$1 < \lambda^{\mathrm{i}} < \lambda^{\mathrm{ii}} < \lambda^{\mathrm{iii}} \tag{74}$$

and the functions taking (η, β, α) to these roots shall be given by $\Phi_{\mathrm{i}}(\eta, \beta, \alpha)$, $\Phi_{\mathrm{ii}}(\eta, \beta, \alpha)$ and $\Phi_{\mathrm{iii}}(\eta, \beta, \alpha)$. Numerical procedures for constructing these functions have been developed and curves of load parameter λ vs ripple parameter η for various values of (β, α) are given in Figs 9–13. Each of the three curves in each figure gives rise to a family of failure load parameters λ owing to the discrete nature of the ripple parameter η as given in $(69)_1$. These shall be denoted by

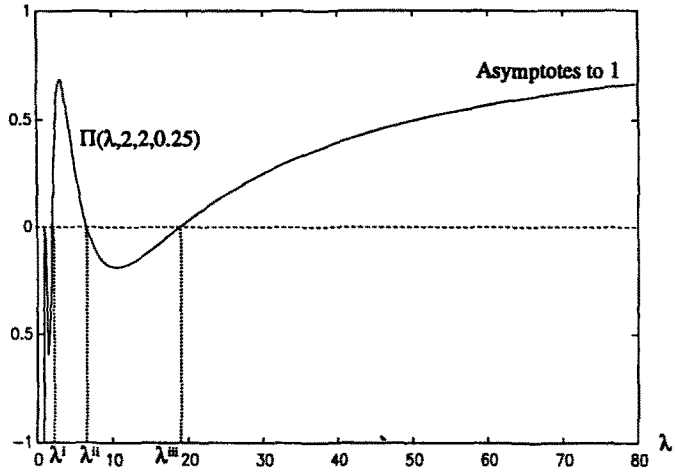

Fig. 8. The two-ply function $\Pi(\lambda, \eta, \beta, \alpha)$ for the case $\eta = 2$, $\beta = 2$, $\alpha = 0.25$. There are three roots, besides $\lambda = 1$, in the two-ply case.

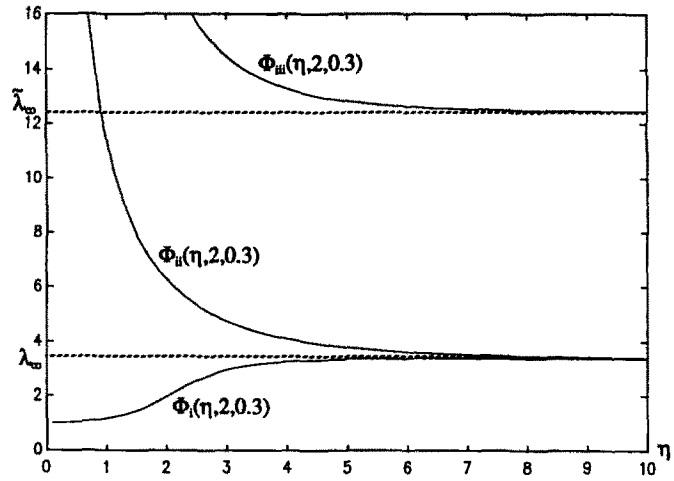

Fig. 9. The functions $\Phi_i(\eta, \beta, \alpha)$, $\Phi_{ii}(\eta, \beta, \alpha)$ and $\Phi_{iii}(\eta, \beta, \alpha)$ for the case $\beta = 2$, $\alpha = 0.3$.

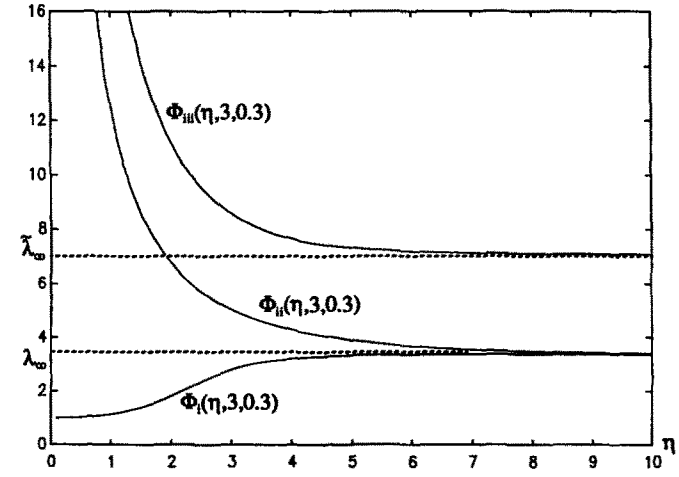

Fig. 10. The functions $\Phi_i(\eta, \beta, \alpha)$, $\Phi_{ii}(\eta, \beta, \alpha)$ and $\Phi_{iii}(\eta, \beta, \alpha)$ for the case $\beta = 3$, $\alpha = 0.3$.

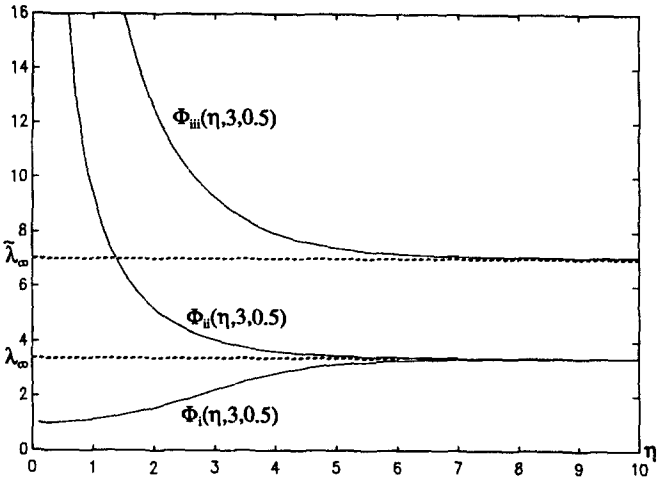

Fig. 11. The functions $\Phi_i(\eta, \beta, \alpha)$, $\Phi_{ii}(\eta, \beta, \alpha)$ and $\Phi_{iii}(\eta, \beta, \alpha)$ for the case $\beta = 3$, $\alpha = 0.5$.

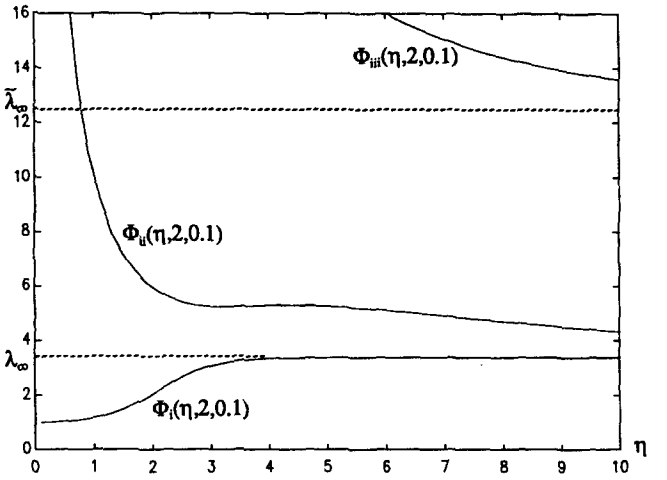

Fig. 12. The functions $\Phi_i(\eta, \beta, \alpha)$, $\Phi_{ii}(\eta, \beta, \alpha)$ and $\Phi_{iii}(\eta, \beta, \alpha)$ for the case $\beta = 2$, $\alpha = 0.1$.

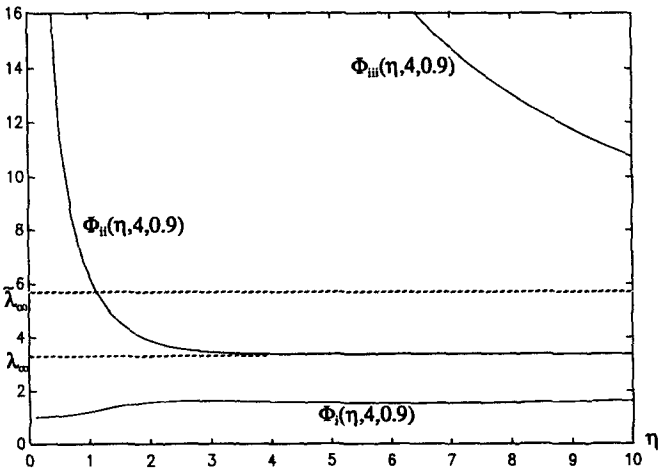

Fig. 13. The functions $\Phi_i(\eta, \beta, \alpha)$, $\Phi_{ii}(\eta, \beta, \alpha)$ and $\Phi_{iii}(\eta, \beta, \alpha)$ for the case $\beta = 4$, $\alpha = 0.9$.

$$\lambda_m^{\mathrm{i}} = \Phi_{\mathrm{i}}(m\pi l_2/l_1, \beta, \alpha),$$
$$\lambda_m^{\mathrm{ii}} = \Phi_{\mathrm{ii}}(m\pi l_2/l_1, \beta, \alpha),$$
$$\lambda_m^{\mathrm{iii}} = \Phi_{\mathrm{iii}}(m\pi l_2/l_1, \beta, \alpha), \quad m = 1, 2, 3 \ldots. \tag{75}$$

The corresponding families of failure thrusts $\{T_m^{\mathrm{i}}, T_m^{\mathrm{ii}}, T_m^{\mathrm{iii}}\}$ with $m = 1, 2, 3, \ldots$ are found from (75) using (14) and $\rho = \lambda^{-1/2}$. It is found as $\eta \to 0$ that the three curves $\Phi_{\mathrm{i}}(\eta, \beta, \alpha)$, $\Phi_{\mathrm{ii}}(\eta, \beta, \alpha)$ and $\Phi_{\mathrm{iii}}(\eta, \beta, \alpha)$ obey

$$\lim_{\eta \to 0} \Phi_{\mathrm{i}}(\eta, \beta, \alpha) = 1, \quad \lim_{\eta \to 0} \Phi_{\mathrm{ii}}(\eta, \beta, \alpha) = \infty, \quad \lim_{\eta \to 0} \Phi_{\mathrm{iii}}(\eta, \beta, \alpha) = \infty. \tag{76}$$

As $\eta \to \infty$ it is found that both $\Phi_{\mathrm{i}}(\eta, \beta, \alpha)$ and $\Phi_{\mathrm{ii}}(\eta, \beta, \alpha)$ approach a common asymptote whereas $\Phi_{\mathrm{iii}}(\eta, \beta, \alpha)$ tends to a different and larger asymptote. The value of these asymptotes can be obtained by a large η analysis of (70) similar to that conducted in Section 3 [viz. eqns (56)–(65)]. To this end it is found that

$$\Psi(\lambda, \eta, \beta, \alpha) \sim \mathrm{e}^{\eta(\lambda+1)} \lambda^{-6} (\lambda - 1)^4 [f_1(\lambda)]^2 f_2(\lambda, \beta), \tag{77}$$

where $f_1(\lambda)$ and $f_2(\lambda, \beta)$ are again given by (61) and (62). Thus

$$\lim_{\eta \to \infty} \Psi_{\mathrm{i}}(\eta, \beta, \alpha) = \lim_{\eta \to \infty} \Psi_{\mathrm{ii}}(\eta, \beta, \alpha) = \lambda_\infty,$$
$$\lim_{\eta \to \infty} \Psi_{\mathrm{iii}}(\eta, \beta, \alpha) = \tilde{\lambda}_\infty(\beta), \tag{78}$$

where λ_∞ and $\tilde{\lambda}_\infty = \tilde{\lambda}_\infty(\beta)$ are again as depicted in Fig. 6. Of the functions $\Phi_{\mathrm{i}}(\eta, \beta, \alpha)$, $\Phi_{\mathrm{ii}}(\eta, \beta, \alpha)$, $\Phi_{\mathrm{iii}}(\eta, \beta, \alpha)$ it follows from a comparison of (76) with (52), (78) with (53), and Figs 9–13 with Figs 4–5 that: $\Phi_{\mathrm{i}}(\eta, \beta, \alpha)$ resembles $\Phi_F(\eta, \beta, \alpha)$, $\Phi_{\mathrm{ii}}(\eta, \beta, \alpha)$ resembles $\Phi_B(\eta, \beta, \alpha)$, and $\Phi_{\mathrm{iii}}(\eta, \beta, \alpha)$ resembles both $\tilde{\Phi}_F(\eta, \beta, \alpha)$ and $\tilde{\Phi}_B(\eta, \beta, \alpha)$. Indeed, as either $\alpha \to 0$, $\alpha \to 1$ or $\beta \to 1$ the functions $\Phi_{\mathrm{i}}(\eta, \beta, \alpha)$ and $\Phi_{\mathrm{ii}}(\eta, \beta, \alpha)$ approach the, respective, lower (flexure) and upper (barrelling) noncomposite curves as given in Fig. 3. Furthermore, since the noncomposite case involves no additional families of buckled solutions, the family of load parameters obtained from $\Phi_{\mathrm{iii}}(\eta, \beta, \alpha)$ will evidently no longer exist if either $\alpha = 0$, $\alpha = 1$ or $\beta = 1$. If $\beta \to 1$ then the asymptote $\tilde{\lambda}_\infty(\beta)$ drags the values $\Phi_{\mathrm{iii}}(\eta, \beta, \alpha)$ to ∞ (compare Figs 10 and 9 which contrast $\beta = 3$ with $\beta = 2$). However if $\alpha \to 0$ or $\alpha \to 1$ with $\beta \neq 1$ then $\tilde{\lambda}_\infty(\beta)$ is finite so that presumably the values $\Phi_{\mathrm{iii}}(\eta, \beta, \alpha)$ tend to ∞ nonuniformly in η (as seen from comparing Figs 9 and 12 for the case $\alpha \to 0$).

The detailed properties of the curves $\Phi_{\mathrm{i}}(\eta, \beta, \alpha)$, $\Phi_{\mathrm{ii}}(\eta, \beta, \alpha)$ and $\Phi_{\mathrm{iii}}(\eta, \beta, \alpha)$ determine the ordering of the failure thrusts T_m^{i}, T_m^{ii} and T_m^{iii} ($m = 1, 2, 3, \ldots$). As in the case of the symmetric three-ply plate, the simplest orderings occur for those parameter pairs (β, α) for which $\Phi_{\mathrm{i}}(\eta, \beta, \alpha)$ is monotonically increasing in η with $\Phi_{\mathrm{ii}}(\eta, \beta, \alpha)$ and $\Phi_{\mathrm{iii}}(\eta, \beta, \alpha)$ monotonically decreasing in η. A detailed study of the monotonicity properties of these functions is not in the scope of the present study. However we do observe from comparing Figs 9–13 for the two-ply construction to Figs 4 and 5 for the symmetric three-ply construction that the two-ply curves appear to be "more monotonic" than the symmetric three-ply curves. However, as shown by Figs 12 and 13, even certain of the two-ply curves may also lose monotonicity. Figures 9–13 also suggest the intriguing result that

$$\Phi_{\mathrm{i}}(\eta, \beta, \alpha) < \lambda_\infty < \Phi_{\mathrm{ii}}(\eta, \beta, \alpha) \quad \text{and} \quad \tilde{\lambda}_\infty < \Phi_{\mathrm{iii}}(\eta, \beta, \alpha). \tag{79}$$

We note from Figs 4 and 5 that such curve separation by asymptotes is not a feature of the symmetric three-ply problem. To inquire further into the validity of (79) we note from $(76)_2$, $(78)_2$ and $\lambda_\infty < \tilde{\lambda}_\infty(\beta)$ that

$$\Phi_{ii}(\eta, \beta, \alpha) - \tilde{\lambda}_{\infty}(\beta) = 0 \tag{80}$$

must have at least one root η. By numerically evaluating $\Psi(\lambda_{\infty}, \eta, \beta, \alpha)$ with varying η and fixed pairs of (β, α), we find no exceptions to the inequality

$$\Psi(\lambda_{\infty}, \eta, \beta, \alpha) > 0. \tag{81}$$

Furthermore by numerically evaluating $\Psi(\tilde{\lambda}_{\infty}, \eta, \beta, \alpha)$ with varying η and fixed pairs of (β, α) we systematically find that there is only one value of $\eta = \eta_{\lambda}$ such that

$$\begin{aligned} &\Psi(\tilde{\lambda}_{\infty}(\beta), \eta, \beta, \alpha) > 0, \quad \text{if } \eta < \eta_{\lambda}; \\ &\Psi(\tilde{\lambda}_{\infty}(\beta), \eta, \beta, \alpha) < 0, \quad \text{if } \eta > \eta_{\lambda}. \end{aligned} \tag{82}$$

So $\eta_{\lambda} = \eta_{\lambda}(\beta, \alpha)$ satisfying

$$\Phi_{ii}(\eta_{\lambda}, \beta, \alpha) - \tilde{\lambda}_{\infty}(\beta) = 0 \tag{83}$$

is, in all cases that we have examined, the unique root of eqn (80). This, in conjunction with $(76)_2$, $(78)_2$, (81) and $\lambda_{\infty} < \tilde{\lambda}_{\infty}(\beta)$, suggests the generality of (79).

The results of this section provide a fairly complete description of the families of plane-strain buckled solutions for the two-ply neo-Hookean laminate construction. A similar description for the (symmetric) three-ply neo-Hookean laminate construction was provided by the results of the previous section. It is tempting to speculate on the possibilities for the families of plane-strain buckled solutions for general N-ply constructions involving alternating plies of two different neo-Hookean materials. We here note that the following *conjecture* is consistent with all of our results: for a composite laminate construction consisting of N alternating plies of two different neo-Hookean materials with shear moduli $\mu^{(I)}$ and $\mu^{(II)}$, we conjecture that there will exist $N+1$ families of plane-strain buckled solutions. Two of these families should involve load parameters λ that asymptote to λ_{∞} as given by (63) and these families should be the extension to the composite case of the solutions obtained by Sawyers and Rivlin (1974). The other $N-1$ families should only exist for genuinely composite constructions and all of them should involve load parameters λ that asymptote to $\tilde{\lambda}_{\infty}(\beta)$ as given by the root of (62) with $\beta = \mu^{(II)}/\mu^{(I)}$. Here we note from (62) that a necessary consistency relation for this conjecture, $\tilde{\lambda}_{\infty}(\beta) = \tilde{\lambda}_{\infty}(\beta^{-1})$, is satisfied.

5. CHARACTERIZATION OF THE DEFORMATION MODES FOR THE TWO-PLY PLATE

In both the noncomposite construction and the symmetric three-ply construction, the construction symmetry with respect to X_2 gives rise to buckled configurations that correspond to either flexure $(U_2(-X_2) = U_2(X_2))$ or barrelling $(U_2(-X_2) = -U_2(X_2))$. However for the two-ply construction, genuinely composite constructions ($\beta \neq 1$, $\alpha \neq 0$ and $\alpha \neq 1$) no longer involve construction symmetry with respect to X_2. Thus, one would anticipate that the associated buckling configurations should exhibit a mixed-mode flexure and barrelling character. It is the purpose of this section to further examine this issue. In the two-ply construction, $U_2(X_2)$ is written as:

$$U_2^{(j)}(X_2) = L_1^{(j)} \cosh(\Omega X_2) + L_2^{(j)} \sinh(\Omega X_2) + M_1^{(j)} \cosh(\lambda\Omega X_2) + M_2^{(j)} \sinh(\lambda\Omega X_2), \tag{84}$$

where $j = 1, 2$ for ply-1 or ply-2, and $\mathbf{l}$ given by (66), can be normalized so that

$$\|\mathbf{l}\|^2 \equiv \mathbf{l}^T\mathbf{l} = 1. \tag{85}$$

Thus the full (linearized) deformation can then be obtained from (15), $(20)_{2,3}$ and $(24)_1$.

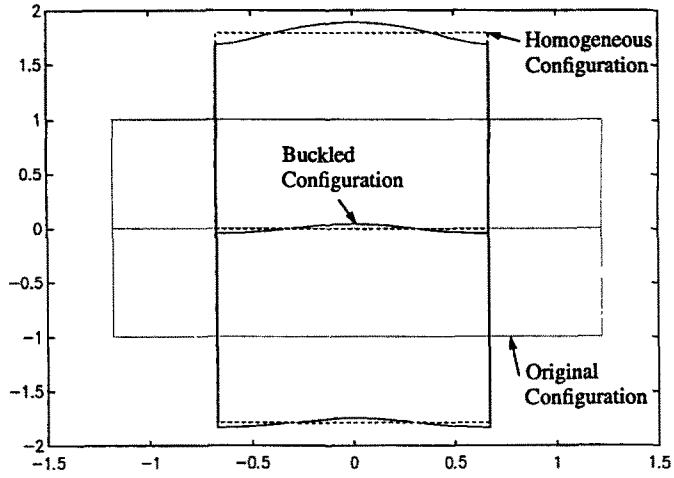

Fig. 14. Deformation of the two-ply composite plate under thrust for $l_1/l_2 = 1.2$, $\varepsilon = 0.1$, $m = 2$ (so that $\eta = m\pi l_2/l_1 = 5.236$), $\beta = 3$, $\alpha = 0.5$. Here the $m = 2$ buckled configuration is from the first family of buckled solutions so that $\lambda = \lambda_2^{\mathrm{I}} = \Phi_{\mathrm{I}}(5.236, 3, 0.5) = 3.199$ (see Fig. 11), and $T = T_2^{\mathrm{I}} = 5.163(\mu^{(\mathrm{I})}\mathrm{A}^{(\mathrm{I})} + \mu^{(\mathrm{II})}\mathrm{A}^{(\mathrm{II})})$.

As an example, we display in Figs 14–16 all three of the deformations for ripple number $m = 2$ associated with the construction $\beta = 3$, $\alpha = 0.5$ and $l_1/l_2 = 1.2$. The corresponding families of solutions to the bifurcation equation (73) were shown previously in Fig. 11. In these deformation figures, the value of the order parameter ε [refer to (15)] is chosen so as to make the deformed configurations distinguishable.

In order to examine the mixed-mode character of the deformation, we decompose the vector $\mathbf{l}$ as follows:

$$\mathbf{l} = \mathbf{a} + \mathbf{b} + \mathbf{c} + \mathbf{d}, \tag{86}$$

$$\mathbf{a} = \{a_1, 0, a_3, 0, a_5, 0, a_7, 0\}^T, \quad \mathbf{b} = \{0, b_2, 0, b_4, 0, b_6, 0, b_8\}^T,$$
$$\mathbf{c} = \{0, c_2, 0, c_4, 0, c_6, 0, c_8\}^T, \quad \mathbf{d} = \{d_1, 0, d_3, 0, d_5, 0, d_7, 0\}^T, \tag{87}$$

where

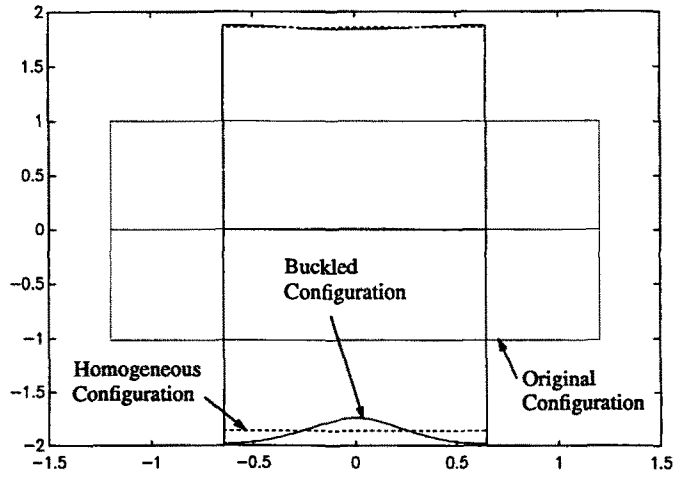

Fig. 15. Deformation of the two-ply composite plate under thrust for $l_1/l_2 = 1.2$, $\varepsilon = 0.05$, $m = 2$ (so that $\eta = m\pi l_2/l_1 = 5.236$), $\beta = 3$, $\alpha = 0.5$. Here the $m = 2$ buckled configuration is from the second family of buckled solutions so that $\lambda = \lambda_2^{\mathrm{II}} = \Phi_{\mathrm{II}}(5.236, 3, 0.5) = 3.457$, and $T = T_2^{\mathrm{II}} = 5.890(\mu^{(\mathrm{I})}\mathrm{A}^{(\mathrm{I})} + \mu^{(\mathrm{II})}\mathrm{A}^{(\mathrm{II})})$.

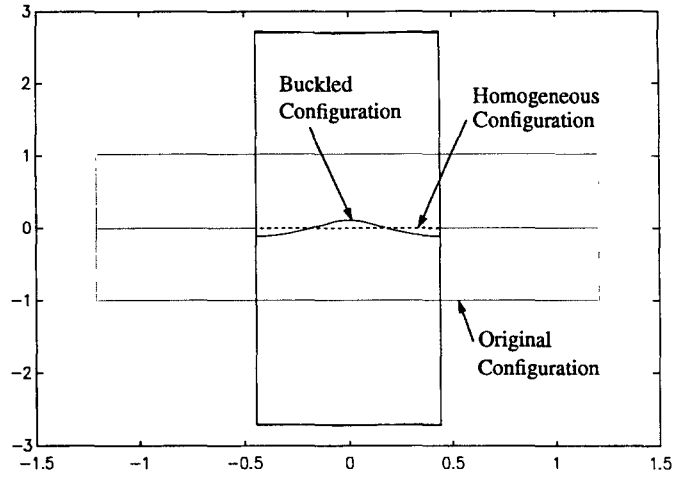

Fig. 16. Deformation of the two-ply composite plate under thrust for $l_1/l_2 = 1.2$, $\varepsilon = 0.3$, $m = 2$ (so that $\eta = m\pi l_2/l_1 = 5.236$), $\beta = 3$, $\alpha = 0.5$. Here the $m = 2$ buckled configuration is from the third family of buckled solutions so that $\lambda = \lambda_2^{\mathrm{III}} = \Phi_{\mathrm{III}}(5.236, 3, 0.5) = 7.345$, and $T = T_2^{\mathrm{III}} = 19.537(\mu^{(\mathrm{I})}\mathrm{A}^{(\mathrm{I})} + \mu^{(\mathrm{II})}\mathrm{A}^{(\mathrm{II})})$.

$$
\begin{aligned}
a_1 = a_5 &= \frac{L_1^{(1)} + L_1^{(2)}}{2}, \quad a_3 = a_7 = \frac{M_1^{(1)} + M_1^{(2)}}{2}, \\
b_2 = b_6 &= \frac{L_2^{(1)} + L_2^{(2)}}{2}, \quad b_4 = b_8 = \frac{M_2^{(1)} + M_2^{(2)}}{2}, \\
c_2 = -c_6 &= \frac{L_2^{(1)} - L_2^{(2)}}{2}, \quad c_4 = -c_8 = \frac{M_2^{(1)} - M_2^{(2)}}{2}, \\
d_1 = -d_5 &= \frac{L_1^{(1)} - L_1^{(2)}}{2}, \quad d_3 = -d_7 = \frac{M_1^{(1)} - M_1^{(2)}}{2}.
\end{aligned} \tag{88}
$$

This decomposition, in the sense of the Euclidean norm used previously in (85), satisfies

$$\|\mathbf{l}\|^2 = \|\mathbf{a}\|^2 + \|\mathbf{b}\|^2 + \|\mathbf{c}\|^2 + \|\mathbf{d}\|^2. \tag{89}$$

By this decomposition, the function $U_2 = U_2(X_2)$ is expressed as

$$U_2 = U_2^a + U_2^b + U_2^c + U_2^d \tag{90}$$

where

$$U_2^a(X_2) = a_1 \cosh(\Omega X_2) + a_3 \cosh(\lambda\Omega X_2), \quad -R_1 \leqslant X_2 \leqslant R_2, \tag{91}$$

$$U_2^b(X_2) = b_2 \sinh(\Omega X_2) + b_4 \sinh(\lambda\Omega X_2), \quad -R_1 \leqslant X_2 \leqslant R_2, \tag{92}$$

$$U_2^c(X_2) = \begin{cases} c_2 \sinh(\Omega X_2) + c_4 \sinh(\lambda\Omega X_2), & -R_1 \leqslant X_2 \leqslant 0, \\ -c_2 \sinh(\Omega X_2) - c_4 \sinh(\lambda\Omega X_2), & 0 \leqslant X_2 \leqslant R_2, \end{cases} \tag{93}$$

$$U_2^d(X_2) = \begin{cases} d_1 \cosh(\Omega X_2) + d_3 \cosh(\lambda\Omega X_2), & -R_1 \leqslant X_2 \leqslant 0, \\ -d_1 \cosh(\Omega X_2) - d_3 \cosh(\lambda\Omega X_2), & 0 \leqslant X_2 \leqslant R_2. \end{cases} \tag{94}$$

Note that the four functions in the decomposition have the following symmetry properties:

$$U_2^a(X_2) = U_2^a(-X_2), \qquad U_2^c(X_2) = U_2^c(-X_2),$$
$$U_2^b(X_2) = -U_2^b(-X_2), \quad U_2^d(X_2) = -U_2^d(-X_2). \tag{95}$$

We shall say that if $\mathbf{b} = \mathbf{0}$ and $\mathbf{d} = \mathbf{0}$, then the whole deformation is one of *pure flexure*; similarly, if $\mathbf{a} = \mathbf{0}$ and $\mathbf{c} = \mathbf{0}$, then the whole deformation is one of *pure barrelling*. The four decomposed deformation portions associated with this decomposition for the example presented in Fig. 14 are displayed in Fig. 17. Since the deformation presented in Fig. 14 was associated with the first buckled family of solutions, i.e. the associated load parameter $\lambda = \lambda^1 = \Phi_1(5.236, 3.0, 0.5) = 3.199$, one might anticipate that flexure would dominate in the decomposition. Indeed one finds in this case that $\|\mathbf{a}\|^2 + \|\mathbf{c}\|^2 = 0.7049$ and $\|\mathbf{b}\|^2 + \|\mathbf{d}\|^2 = 0.2951$. Similarly, Fig. 18 gives the four decomposed deformations for the example presented in Fig. 15. Since this deformation is associated with the second buckled family of solutions one might anticipate that barrelling would predominate. Indeed for this example one finds that $\|\mathbf{a}\|^2 + \|\mathbf{c}\|^2 = 0.3859$ and $\|\mathbf{b}\|^2 + \|\mathbf{d}\|^2 = 0.6141$.

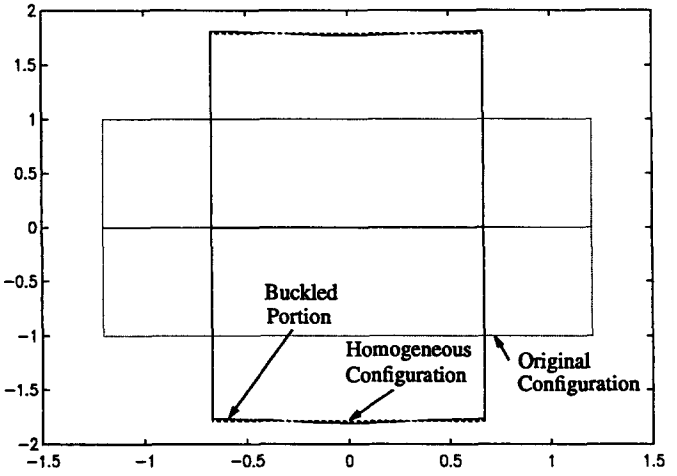

Fig. 17a. The smooth flexural deformation portion at $\varepsilon = 0.0001$, $m = 2$, $\eta = 5.236$, $\beta = 3.0$, $\alpha = 0.5$, $\lambda = \Phi_1(5.236, 3.0, 0.5) = 3.199$. Here $\|\mathbf{a}\|^2 = 0.5317$. The overall deformation was shown previously in Fig. 14.

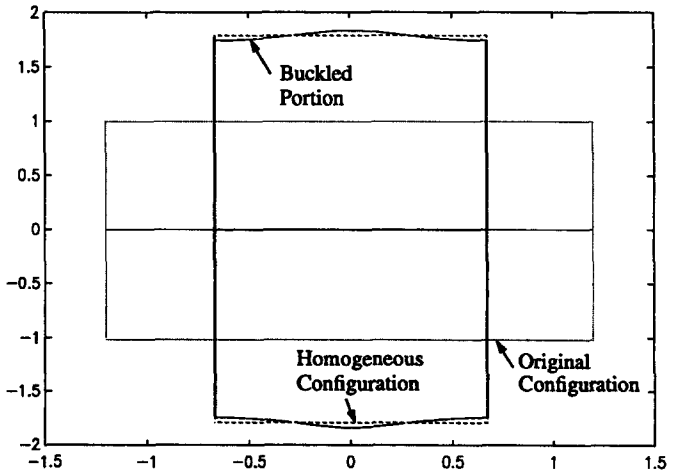

Fig. 17b. The smooth barrelling deformation portion at $\varepsilon = 0.0001$, $m = 2$, $\eta = 5.236$, $\beta = 3.0$, $\alpha = 0.5$, $\lambda = \Phi_1(5.236, 3.0, 0.5) = 3.199$. Here $\|\mathbf{b}\|^2 = 0.1166$. The overall deformation was shown previously in Fig. 14.

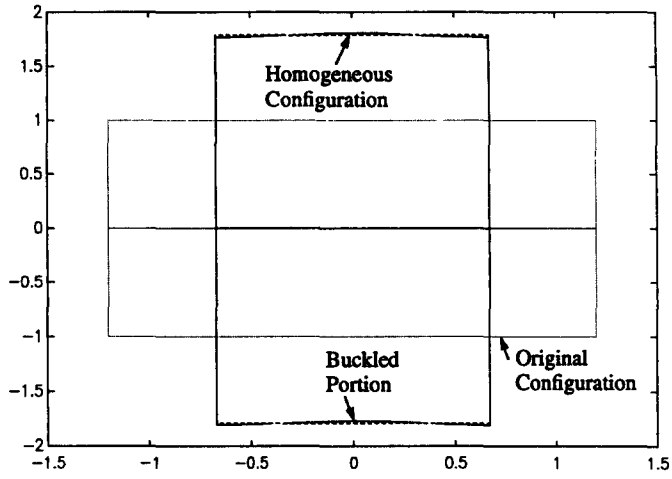

Fig. 17c. The residual flexural deformation portion at $\varepsilon = 0.0001, m = 2, \eta = 5.236, \beta = 3.0, \alpha = 0.5$, $\lambda = \Phi_1(5.236, 3.0, 0.5) = 3.199$. Here $\|\mathbf{c}\|^2 = 0.1732$. The overall deformation was shown previously in Fig. 14.

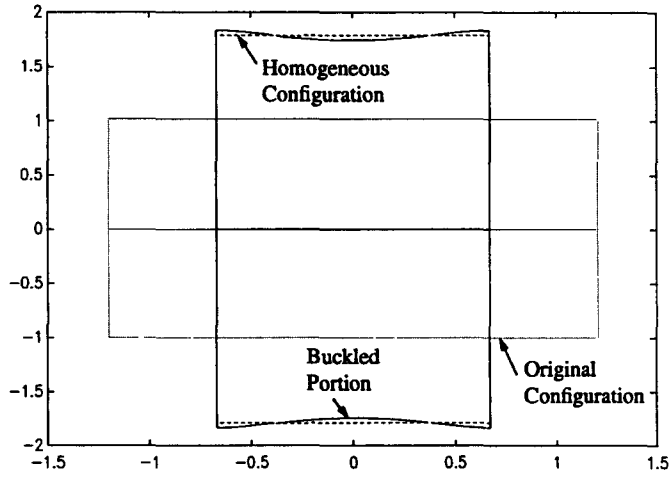

Fig. 17d. The residual barrelling deformation portion at $\varepsilon = 0.0001$, $m = 2$, $\eta = 5.236$, $\beta = 3.0$, $\alpha = 0.5$, $\lambda = \Phi_1(5.236, 3.0, 0.5) = 3.199$. Here $\|\mathbf{d}\|^2 = 0.1785$. The overall deformation was shown previously in Fig. 14.

The four decomposed deformation portions can, as we now show, be used to characterize the interfacial deformation smoothness discontinuity at the ply interface $X_2 = 0$. For this purpose it is convenient to introduce the notation $[[\ ]]|_0$ to indicate the jump in value across this interface. Clearly from (91), (92) it follows that

$$[[(U_2^a)^{(n)}]]|_0 = 0, \quad [[(U_2^b)^{(n)}]]|_0 = 0, \tag{96}$$

for $n = 0, 1, 2, 3, \ldots$. Here (n) denotes a derivative of order n with (0) indicating the undifferentiated function. Similarly (91) and (92) also directly give that

$$[[(U_2^c)^{(2n)}]]|_0 = 0, \quad [[(U_2^d)^{(2n+1)}]]|_0 = 0, \tag{97}$$

for $n = 0, 1, 2, 3, \ldots$, where the derivatives appearing in (97) are standard one-sided derivatives. To address the possible discontinuity in the (one-sided) derivatives $(U_2^c)^{(2n+1)}$ and $(U_2^d)^{(2n)}$ at the interface $X_2 = 0$, we note that the interface conditions (9) with (19) give the following conditions, respectively, on $U_2(X_2)$ and $U_2'(X_2)$:

$$[[U_2]]|_0 = 0, \quad [[U_2']]|_0 = 0, \tag{98}$$

which along with (96), (97) give

$$[[(U_2^c)^{(1)}]]|_0 = 0, \quad [[(U_2^d)^{(0)}]]|_0 = 0. \tag{99}$$

However $(U_2^c)^{(2n+1)}$, $(U_2^d)^{(2n)}$ for $n = 1, 2, 3, \ldots$ are not continuous across the interface $X_2 = 0$.

Thus by using the boundary and interface conditions, we conclude, for $-R_1 \leqslant X_2 \leqslant R_2$, that U_2^a and U_2^b and their derivatives of any order are continuous; $(U_2^c)^{(0)}$, $(U_2^c)^{(1)}$ and $(U_2^c)^{(2n)}$ are continuous, and $(U_2^d)^{(0)}$, $(U_2^d)^{(1)}$ and $(U_2^d)^{(2n+1)}$ are continuous. Furthermore one obtains from (90)–(94) that

$$[[U_2^{(2n)}]]|_0 = [[(U_2^d)^{(2n)}]]|_0 = -2(\Omega^{2n} d_1 + (\lambda\Omega)^{2n} d_3), \tag{100}$$

$$[[U_2^{(2n+1)}]]|_0 = [[(U_2^c)^{(2n+1)}]]|_0 = -2(\Omega^{2n+1} c_2 + (\lambda\Omega)^{2n+1} c_4), \tag{101}$$

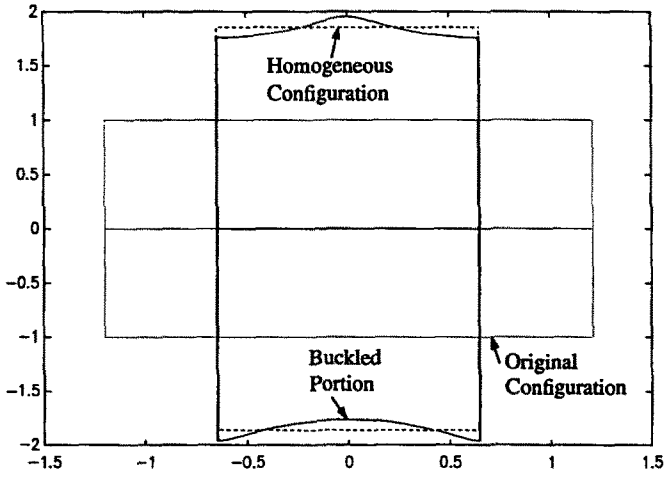

Fig. 18a. The smooth flexural deformation portion at $\varepsilon = 0.0002$, $m = 2$, $\eta = 5.236$, $\beta = 3.0$, $\alpha = 0.5$, $\lambda = \Phi_{\mathrm{II}}(5.236, 3.0, 0.5) = 3.457$. Here $\|\mathbf{a}\|^2 = 0.0357$. The overall deformation was shown previously in Fig. 15.

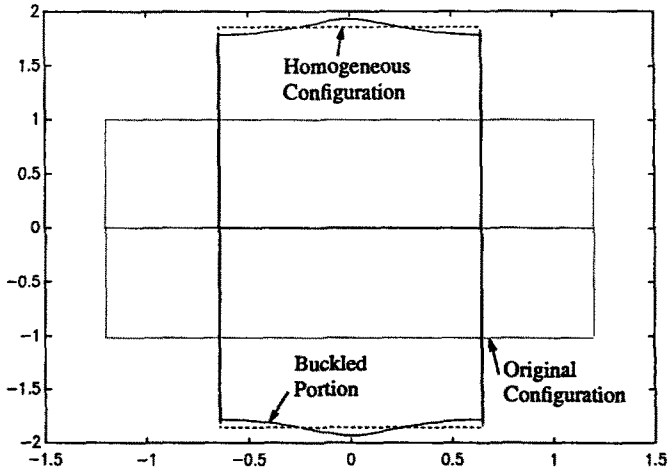

Fig. 18b. The smooth barrelling deformation portion at $\varepsilon = 0.0002$, $m = 2$, $\eta = 5.236$, $\beta = 3.0$, $\alpha = 0.5$, $\lambda = \Phi_{\mathrm{II}}(5.236, 3.0, 0.5) = 3.457$. Here $\|\mathbf{b}\|^2 = 0.5835$. The overall deformation was shown previously in Fig. 15.

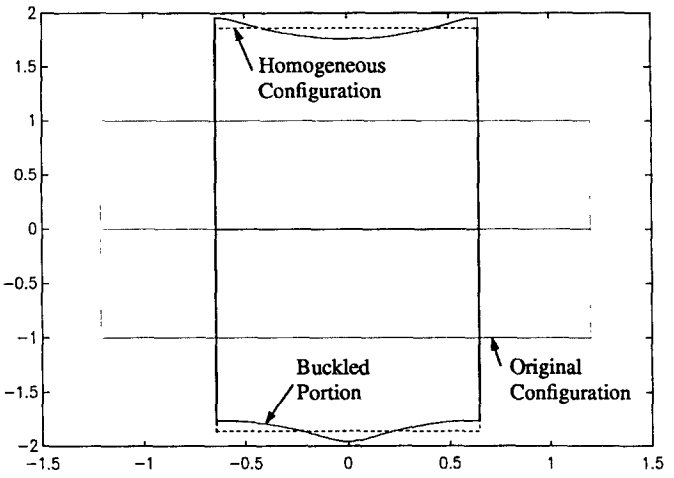

Fig. 18c. The residual flexural deformation portion at $\varepsilon = 0.0002$, $m = 2$, $\eta = 5.236$, $\beta = 3.0$, $\alpha = 0.5$, $\lambda = \Phi_{11}(5.236, 3.0, 0.5) = 3.457$. Here $\|\mathbf{c}\|^2 = 0.3502$. The overall deformation was shown previously in Fig. 15.

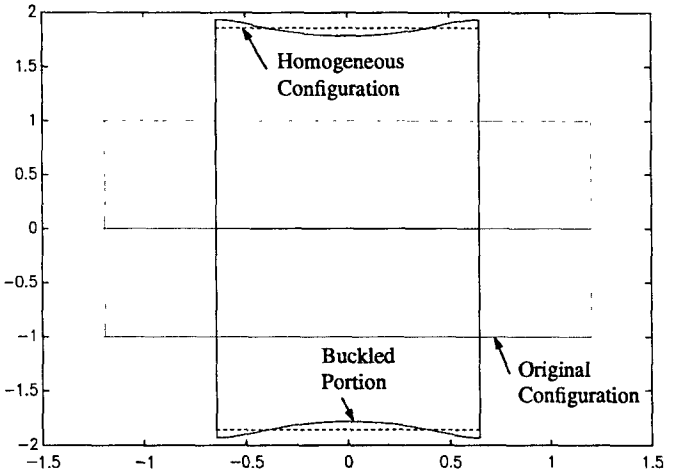

Fig. 18d. The residual barrelling deformation portion at $\varepsilon = 0.0002$, $m = 2$, $\eta = 5.236$, $\beta = 3.0$, $\alpha = 0.5$, $\lambda = \Phi_{11}(5.236, 3.0, 0.5) = 3.457$. Here $\|\mathbf{d}\|^2 = 0.0306$. The overall deformation was shown previously in Fig. 15.

where $n = 1, 2, 3, \ldots$, and a superscript number n inside parentheses indicates the nth derivative, and a superscript number n without parentheses indicates exponentiation to the power of n. In view of the preceding discussion, we shall refer to $U_2^a(X_2)$ as the *smooth flexure* part of the decomposition, $U_2^b(X_2)$ as the *smooth barrelling* part, $U_2^c(X_2)$ as the *residual flexure* part, and $U_2^d(X_2)$ as the *residual barrelling* part.

According to (96), (94) and (99), we have

$$d_1 + d_3 = 0 \quad \text{and} \quad c_2 + \lambda c_4 = 0. \tag{102}$$

With eqn (102), by using the interface continuity condition (98), we find that

$$d_1 = \frac{D_1}{D} a_1 + \frac{D_2}{D} a_3 \quad \text{and} \quad c_2 = -\frac{D_2}{D} b_2 - \frac{\lambda D_1}{D} b_4, \tag{103}$$

where

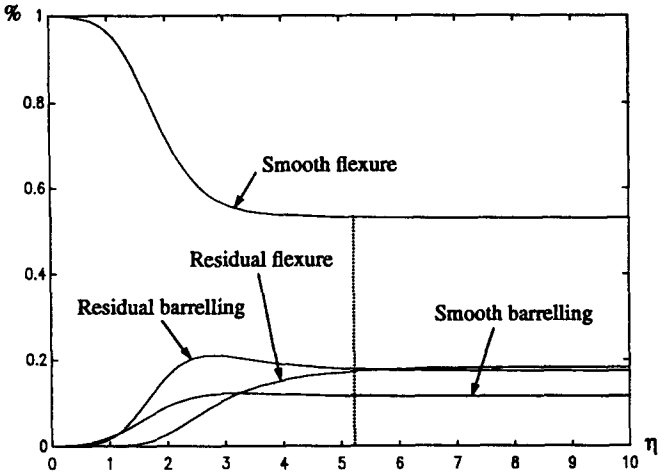

Fig. 19. The four deformation percentages as they vary with η for the case of $\beta = 3$, $\alpha = 0.5$, associated with the first root $\lambda^{i} = \Phi_{i}(\eta, 3.0, 0.5)$ of the buckling equation (73). The vertical line at $\eta = 5.236$ provides correlation with Fig. 17.

$$D = (\beta+1)(1-\lambda^2), \quad D_1 = (\beta-1)(1+\lambda^2), \quad D_2 = 2(\beta-1)\lambda^2. \tag{104}$$

On account of (88), (95), (102)–(104), we conclude that if the deformation is one of pure flexure, then $c_2 = c_4 = c_6 = c_8 = 0$ so that it is in fact smooth flexure. Similarly, if the deformation is one of pure barrelling, then it is in fact smooth barrelling.

Under the normalization (85), the values $\|\mathbf{a}\|^2$, $\|\mathbf{b}\|^2$, $\|\mathbf{c}\|^2$ and $\|\mathbf{d}\|^2$ correspond to the percentage of smooth flexure, smooth barrelling, residual flexure and residual barrelling within the overall buckled deformation. We find, for a given two-ply construction characterized by a particular (β, α), that these four deformation type percentages vary with ripple parameter η. Figure 19 displays these changing percentages for the first buckled family of solutions for the case $\beta = 3$, $\alpha = 0.5$. Similarly Fig. 20 gives these changing percentages for the second buckled family of solutions, here however we only depict values of $\eta \geqslant 1$ in view of numerical difficulties associated with the large values of λ for this family near $\eta = 0$ [see $(76)_2$]. These numerical difficulties also prevented us from calculating these percentages for the third buckled family of solutions. As anticipated, smooth flexure is dominant for the first buckling family, depicted in Fig. 19. We note, however, that this

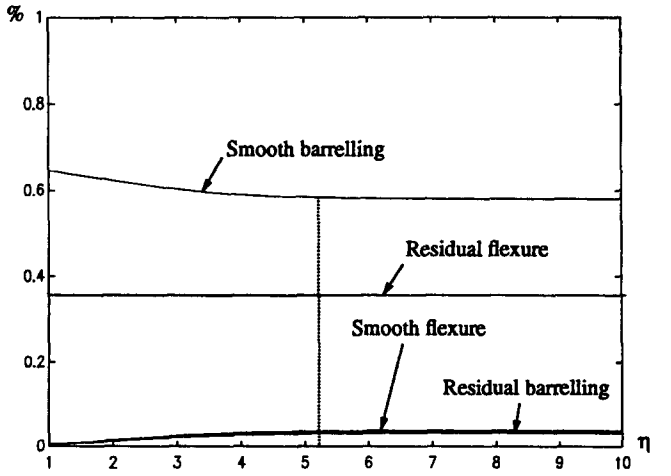

Fig. 20. The four deformation percentages as they vary with η for the case of $\beta = 3$, $\alpha = 0.5$, associated with the second root $\lambda^{ii} = \Phi_{ii}(\eta, 3.0, 0.5)$ of the buckling equation (73). The vertical line at $\eta = 5.236$ provides correlation with Fig. 18.

dominance lessens as the ripple parameter η increases, resulting in a percentage growth of both the smooth barrelling percentage and the residual deformation types. Similarly, as one would anticipate, the smooth barrelling percentage dominates the second buckling family, depicted in Fig. 20, with a percentage growth in the other deformation percentages for increasing η.

Acknowledgements—This work was supported by the Composite Materials and Structures Center, Michigan State University, under the REF program, and by the U.S. Army Research Office through Grant DAAL 03-89-G-0089.

REFERENCES

Biot, M. A. (1965). *Mechanics of Incremental Deformations*. John Wiley & Sons, New York.
Biot, M. A. (1968). Edge buckling of a laminated medium. *Int. J. Solids Structures* **4**, 125–137.
Pence, T. J. and Song, J. (1991). Buckling instabilities in a thick elastic three-ply composite plate under thrust. *Int. J. Solids Structures* **27**, 1809–1828.
Qiu, Y. (1992). Buckling of a two-ply nonlinear elastic plate. Master Thesis, Department of Materials Science and Mechanics, Michigan State University.
Sawyers, K. N. and Rivlin, R. S. (1974). Bifurcation conditions for a thick elastic plate under thrust. *Int. J. Solids Structures* **10**, 483–501.
Sawyers, K. N. and Rivlin, R. S. (1982). Stability of a thick elastic plate under thrust. *J. Elasticity* **12**, 101–124.
Song, J. and Pence, T. J. (1992). On the design of three-ply nonlinearly elastic composite plates with optimal resistance to buckling. *Structural Optimization* **5**, 45–54.

APPENDIX A: THE EXPRESSION $\Psi_*(\lambda, \eta, \beta, \alpha)$ FOR THE SYMMETRIC THREE-PLY PLATE

Both the flexural and barrelling determinant, $\Psi_*(\lambda, \eta, \beta, \alpha)$, for the symmetric three-ply plate as given in (32) and (33) can be expressed as

$$\Psi_*(\lambda, \eta, \beta, \alpha) = \tfrac{1}{8}\mathbf{H}_*\mathbf{P}\Lambda, \tag{A.1}$$

where

$$\mathbf{H}_* = \mathbf{H}_*(\lambda, \eta, \alpha)_{1\times 10} = \{\sinh(\eta\kappa_1), \sinh(\eta\kappa_2), \ldots, \sinh(\eta\kappa_{10})\}, \tag{A.2}$$

$$\mathbf{P} = [P_{i,j}(\beta)]_{10\times 10}, \tag{A.3}$$

$$\Lambda = \Lambda(\lambda)_{10\times 1} = \{\lambda^{-4}, \lambda^{-3}, \ldots, \lambda^{0}, \ldots, \lambda^{4}, \lambda^{5}\}^T. \tag{A.4}$$

The $\kappa_i = \kappa_i(\lambda, \alpha)$ $(i = 1, 2, \ldots, 10)$ in (A.2) have different values for the flexure and barrelling cases, but by using the exchange rule (38), one can convert between these two cases. The κ_is for the flexural deformation are given by:

$$\begin{aligned}
&\kappa_1 = \lambda+1, \quad \kappa_2 = \lambda-1,\\
&\kappa_3 = \lambda+2\alpha-1, \quad \kappa_4 = \lambda-2\alpha+1,\\
&\kappa_5 = 2\alpha\lambda-\lambda+1, \quad \kappa_6 = 2\alpha\lambda-\lambda-1,\\
&\kappa_7 = 2\alpha\lambda+2\alpha-\lambda-1 = (\lambda+1)(2\alpha-1),\\
&\kappa_8 = 2\alpha\lambda-2\alpha-\lambda+1 = (\lambda-1)(2\alpha-1),\\
&\kappa_9 = \lambda\alpha+\alpha = (\lambda+1)\alpha, \quad \kappa_{10} = \lambda\alpha-\alpha = (\lambda-1)\alpha,
\end{aligned} \tag{A.5}$$

and after exchanging $1 \leftrightarrow \lambda$, and $\alpha \leftrightarrow \alpha\lambda$ in the expanded forms of (A.5), one obtains for the barrelling deformation that

$$\begin{aligned}
&\kappa_1 = \lambda+1, \quad \kappa_2 = -(\lambda-1),\\
&\kappa_3 = 2\alpha\lambda-\lambda+1, \quad \kappa_4 = -(2\alpha\lambda-\lambda-1),\\
&\kappa_5 = \lambda+2\alpha-1, \quad \kappa_6 = -(\lambda-2\alpha+1),\\
&\kappa_7 = 2\alpha+2\alpha\lambda-1-\lambda = (\lambda+1)(2\alpha-1),\\
&\kappa_8 = 2\alpha-2\alpha\lambda-1+\lambda = -(\lambda-1)(2\alpha-1),\\
&\kappa_9 = (\lambda+1)\alpha, \quad \kappa_{10} = -(\lambda-1)\alpha.
\end{aligned} \tag{A.6}$$

Table A.1. The elements of the matrix **P** of (41) for the symmetric three-ply plate

i \ j	−4	−3	−2	−1	0	1	2	3	4	5
1	*	*	$-4P_{1,-3}$	*	*	*	$-36P_{1,-3}$	*	*	$P_{1,-3}$
2	$P_{1,4}$	$-P_{1,-3}$	$-4P_{1,-3}$	$-P_{1,-1}$	$P_{1,0}$	$-P_{1,1}$	$-36P_{1,-3}$	$-P_{1,3}$	$P_{1,4}$	$-P_{1,-3}$
3	*	$-P_{1,-3}$	$4P_{3,-4}$	$4P_{3,-4}$	*	*	$-2P_{3,0}$	$-12P_{3,-4}$	*	$-P_{1,-3}$
4	$P_{3,-4}$	$P_{1,-3}$	$4P_{3,-4}$	$-4P_{3,-4}$	$P_{3,0}$	$-P_{3,1}$	$-2P_{3,0}$	$12P_{3,-4}$	$P_{3,4}$	$P_{1,-3}$
5	$P_{3,-4}$	$-P_{1,-3}$	$4P_{3,-4}$	$4P_{3,-4}$	$P_{3,0}$	$P_{3,1}$	$-2P_{3,0}$	$-12P_{3,-4}$	$P_{3,4}$	$-P_{1,-3}$
6	$P_{3,-4}$	$P_{1,-3}$	$4P_{3,-4}$	$-4P_{3,-4}$	$P_{3,0}$	$-P_{3,1}$	$-2P_{3,0}$	$12P_{3,-4}$	$P_{3,4}$	$P_{1,-3}$
7	$-P_{1,-3}$	$P_{1,-3}$	$-4P_{1,-3}$	$12P_{1,-3}$	$-14P_{1,-3}$	$22P_{1,-3}$	$-36P_{1,-3}$	$28P_{1,-3}$	$-9P_{1,-3}$	$P_{1,-3}$
8	$-P_{1,-3}$	$-P_{1,-3}$	$-4P_{1,-3}$	$-12P_{1,-3}$	$-14P_{1,-3}$	$-22P_{1,-3}$	$-36P_{1,-3}$	$-28P_{1,-3}$	$-9P_{1,-3}$	$-P_{1,-3}$
9	0	0	*	*	*	$-64P_{1,-3}$	*	*	*	0
10	0	0	$P_{9,-2}$	$-P_{9,-1}$	$P_{9,0}$	$64P_{1,-3}$	$P_{9,2}$	$-P_{9,3}$	$P_{9,4}$	0

Each element of the 10×10 matrix **P** is a multiple of one of 17 distinctive polynomials which are denoted by * in Table A.1. Here, and in what follows, the column index j of the matrix entry $P_{i,j}$ is offset by -5 for consistency with the exponents of λ given in (A.4). The 17 distinctive $P_{i,j}(\beta)$s are given by:

$$P_{1,-4}(\beta) = -(\beta+1)^2, \qquad P_{1,-3}(\beta) = (\beta-1)^2,$$

$$P_{1,-1}(\beta) = 4(3\beta^2-2\beta+3), \qquad P_{1,0}(\beta) = -2(7\beta^2-18\beta+7),$$

$$P_{1,1}(\beta) = 2(11\beta^2-38\beta+11), \qquad P_{1,3}(\beta) = 4(7\beta^2-10\beta+7),$$

$$P_{1,4}(\beta) = -(9\beta^2-14\beta+9), \qquad P_{3,-4}(\beta) = -(\beta-1)(\beta+1),$$

$$P_{3,0}(\beta) = -2(\beta-1)(3\beta-1), \qquad P_{3,1}(\beta) = -2(\beta-1)(3\beta+5),$$

$$P_{3,4}(\beta) = -(\beta-1)(\beta-7), \qquad P_{9,-2}(\beta) = 16\beta(\beta-1),$$

$$P_{9,-1}(\beta) = 32(\beta-1), \qquad P_{9,0}(\beta) = 16(\beta-1)(3\beta-2),$$

$$P_{9,2}(\beta) = 16(\beta-1)(3\beta-4), \qquad P_{9,3}(\beta) = -32(\beta-1)(2\beta-1),$$

$$P_{9,4}(\beta) = 16(\beta-1)(\beta-2).$$

APPENDIX B: THE EXPRESSION $\Psi(\lambda, \eta, \beta, \alpha)$ FOR THE TWO-PLY PLATE

$\Psi(\lambda, \eta, \beta, \alpha)$ can be expressed as

$$\Psi(\lambda, \eta, \beta, \alpha) = \tfrac{1}{8}\mathbf{HP}\Lambda, \tag{B.1}$$

where

$$\Lambda = \{\lambda^{-6}, \lambda^{-5}, \ldots, \lambda^0, \ldots, \lambda^6, \lambda^7\}^T, \tag{B.2}$$

$$\mathbf{H} = \mathbf{H}(\lambda, \eta, \alpha) = \{\cosh(\eta\kappa_0), \cosh(\eta\kappa_1), \ldots, \cosh\eta\kappa_{12})\}, \tag{B.3}$$

and **P** is a 13 by 14 matrix with entires $P_{i,j}(\beta)$

$$\mathbf{P} = [P_{i,j}(\beta)]_{13\times 14}. \tag{B.4}$$

The $\kappa_i = \kappa_i(\lambda, \alpha)$ $(i = 0, \ldots, 12)$ are given by

$$\kappa_0 = 0, \tag{B.5}$$

$$\kappa_1 = (\lambda+1), \qquad \kappa_2 = (\lambda+2\alpha-1),$$

$$\kappa_3 = (\lambda-2\alpha+1), \qquad \kappa_4 = (\lambda-1),$$

$$\kappa_5 = (2\alpha\lambda-\lambda+1), \qquad \kappa_6 = (\lambda+1)(2\alpha-1),$$

$$\kappa_7 = (\lambda-1)(2\alpha-1), \qquad \kappa_8 = (2\alpha\lambda-\lambda-1),$$

$$\kappa_9 = (\lambda+1)\alpha, \qquad \kappa_{10} = (\lambda-1)\alpha,$$

$$\kappa_{11} = (\lambda+1)(1-\alpha), \qquad \kappa_{12} = (\lambda-1)(1-\alpha).$$

Table B.1. The elements of the matrix **P** of (B.1) for the two-ply plate

i \ j	-6	-5	-4	-3	-2	-1	0
0	0	0	0	*	0	$256P_{4,7}$	0
1	$-P_{4,-6}$	$P_{4,7}$	$-P_{4,-4}$	$P_{4,-3}$	$-P_{4,-2}$	$63P_{4,7}$	$-P_{4,0}$
2	*	$-P_{4,7}$	$6P_{2,-4}$	$-2P_{4,7}$	$11P_{2,-6}$	$P_{4,7}$	$-12P_{2,-6}$
3	$-P_{2,-6}$	$-P_{4,7}$	$-6P_{2,-4}$	$-2P_{4,7}$	$-11P_{2,-6}$	$P_{4,7}$	$12P_{2,-6}$
4	*	$P_{4,7}$	*	*	*	$63P_{4,7}$	*
5	$P_{2,-6}$	$-P_{4,7}$	$6P_{2,-4}$	$-2P_{4,7}$	$11P_{2,-6}$	$P_{4,7}$	$-12P_{2,-6}$
6	$-P_{4,7}$	$P_{4,7}$	$-6P_{4,7}$	$18P_{4,7}$	$-27P_{4,7}$	$63P_{4,7}$	$-116P_{4,7}$
7	$P_{4,7}$	$P_{4,7}$	$6P_{4,7}$	$18P_{4,7}$	$27P_{4,7}$	$63P_{4,7}$	$116P_{4,7}$
8	$-P_{2,-6}$	$-P_{4,7}$	$-6P_{2,-4}$	$-2P_{4,7}$	$-11P_{2,-6}$	$P_{4,7}$	$12P_{2,-6}$
9	0	0	*	$-2P_{11,-4}$	*	$-128P_{4,7}$	*
10	0	0	$-P_{9,-4}$	$-2P_{11,-4}$	$-P_{9,-2}$	$-128P_{4,7}$	$-P_{9,0}$
11	0	0	*	$-2P_{9,-4}$	*	$-128P_{4,7}$	*
12	0	0	$-P_{11,-4}$	$-2P_{9,-4}$	$-P_{11,-2}$	$-128P_{4,7}$	$-P_{11,0}$

i \ j	1	2	3	4	5	6	7
0	*	0	$768P_{4,7}$	0	*	0	0
1	$P_{4,1}$	$-P_{4,2}$	$223P_{4,7}$	$-P_{4,4}$	$P_{4,5}$	$-P_{4,6}$	$P_{4,7}$
2	$20P_{4,7}$	$-41P_{2,-6}$	$-31P_{4,7}$	$38P_{2,-6}$	$14P_{4,7}$	$-3P_{2,-6}$	$-P_{4,7}$
3	$20P_{4,7}$	$41P_{2,-6}$	$-31P_{4,7}$	$-38P_{2,-6}$	$14P_{4,7}$	$3P_{2,-6}$	$-P_{4,7}$
4	*	*	$223P_{4,7}$	*	*	*	*
5	$20P_{4,7}$	$-41P_{2,-6}$	$-31P_{4,7}$	$38P_{2,-6}$	$14P_{4,7}$	$-3P_{2,-6}$	$-P_{4,7}$
6	$140P_{4,7}$	$-183P_{4,7}$	$223P_{4,7}$	$-166P_{4,7}$	$66P_{4,7}$	$-13P_{4,7}$	$P_{4,7}$
7	$140P_{4,7}$	$183P_{4,7}$	$223P_{4,7}$	$166P_{4,7}$	$66P_{4,7}$	$13P_{4,7}$	$P_{4,7}$
8	$20P_{4,7}$	$41P_{2,-6}$	$-31P_{4,7}$	$-38P_{2,-6}$	$14P_{4,7}$	$3P_{2,-6}$	$-P_{4,7}$
9	*	*	$-384P_{4,7}$	*	*	*	0
10	$P_{9,1}$	$-P_{9,2}$	$-384P_{4,7}$	$-P_{9,4}$	$P_{9,5}$	$-P_{9,6}$	0
11	*	*	$-384P_{4,7}$	*	*	*	0
12	$P_{11,1}$	$-P_{11,2}$	$-384P_{4,7}$	$-P_{11,4}$	$P_{11,5}$	$-P_{11,6}$	0

The particular values for the $P_{i,j}(\beta)$s are given in Table B.1 [in terms of 31 distinctive $P_{i,j}(\beta)$s that are denoted by *]. The 31 distinctive $P_{i,j}(\beta)$s are:

$$P_{0,-3} = -64\beta, \qquad P_{0,1} = 768\beta^2 - 1408\beta + 768,$$
$$P_{0,5} = 256\beta^2 - 578\beta + 256, \qquad P_{2,-6} = \beta^2 - 1,$$
$$P_{4,-6} = \beta^2 + 2\beta + 1, \qquad P_{4,-4} = 6\beta^2 - 4\beta + 6,$$
$$P_{4,-3} = 18\beta^2 - 4\beta + 18, \qquad P_{4,-2} = 27\beta^2 - 58\beta + 27,$$
$$P_{4,0} = 116\beta^2 - 184\beta + 116, \qquad P_{4,1} = 140\beta^2 - 344\beta + 140,$$
$$P_{4,2} = 183\beta^2 - 498\beta + 183, \qquad P_{4,4} = 166\beta^2 - 260\beta + 166,$$
$$P_{4,5} = 66\beta^2 - 100\beta + 66, \qquad P_{4,6} = 13\beta^2 - 22\beta + 13,$$
$$P_{4,7} = \beta^2 - 2\beta + 1, \qquad P_{9,-4} = -16\beta + 16,$$
$$P_{9,-2} = 32\beta^2 - 112\beta + 80, \qquad P_{9,0} = 256\beta^2 - 416\beta + 160,$$
$$P_{9,1} = -320\beta^2 + 704\beta - 384, \qquad P_{9,2} = 448\beta^2 - 864\beta + 416,$$
$$P_{9,4} = 256\beta^2 - 592\beta + 336, \qquad P_{9,5} = -160\beta^2 + 288\beta - 128,$$
$$P_{9,6} = 32\beta^2 - 48\beta + 16, \qquad P_{11,-4} = 16\beta^2 - 16\beta,$$
$$P_{11,-2} = 80\beta^2 - 112\beta + 32, \qquad P_{11,0} = 160\beta^2 - 416\beta + 256,$$
$$P_{11,1} = -384\beta^2 + 704\beta - 320, \qquad P_{11,2} = 416\beta^2 - 864\beta + 448,$$
$$P_{11,4} = 336\beta^2 - 592\beta + 256, \qquad P_{11,5} = -128\beta^2 + 288\beta - 160,$$
$$P_{11,6} = 16\beta^2 - 48\beta + 32.$$